



Garnet growth across the quartz–coesite transition in metapelites: equilibrium vs. kinetics

Paola Manzotti¹, Federica Schiavi², Michel Ballèvre³, and Francesco Nosenzo¹

¹Department of Geological Sciences, Stockholm University, Stockholm, 106 91, Sweden

²Université Clermont-Auvergne, CNRS, IRD, OPGC, Laboratoire Magmas et Volcans, Clermont-Ferrand, 63000, France

³Geosciences Rennes, University of Rennes, Rennes, 35830, France

Correspondence: Paola Manzotti (paola.manzotti@geo.su.se)

Received: 11 March 2025 – Revised: 8 May 2025 – Accepted: 9 May 2025 – Published: 21 July 2025

Abstract. This study explores the growth of garnet across the quartz–coesite transition in metapelite. Garnet chemistry and texture were investigated in several metapelite samples (garnet–chloritoid micaschist) collected across different units in the northern Dora-Maira Massif (Western Alps), and thermodynamic modelling was used to constrain the P – T (pressure and temperature) conditions of garnet growth. Two groups of garnet–chloritoid micaschist were identified.

The first one displays evidence for a single garnet generation (Alpine in age) and occurs both in the basement (Muret Unit and Chasteiran Unit) and cover (Serre Unit) of the northern Dora-Maira Massif. In these rocks, garnet crystals display similar texture, chemistry, and P – T conditions of nucleation and growth. Coesite is found as tiny inclusions in the garnet outer cores. Thermodynamic modelling indicates that garnet cores (alm₇₆prp₆grs_{5–6}) nucleated in the quartz stability field or at the quartz–coesite transition at 2.5–2.7 GPa and 470–530 °C. Its growth (alm_{78–80}prp_{8–10}grs_{5–6}) culminated at 2.9–3.0 GPa and 530–550 °C in the coesite–chloritoid stability field. Peak burial conditions are very similar from sample to sample, irrespective of the unit where they occur, and samples were modelled in P – T conditions of 0.1 GPa and 20 °C. These P – T values are considered to be within the uncertainties accepted for thermodynamic modelling, suggesting that overstepping did not play a major role during garnet formation. A second stage of garnet growth (garnet rim), characterized by a sharp increase in grossular (up to 26 mol %) and decrease in pyrope (up to 3 mol %) is commonly observed: it developed during decompression in the quartz stability field (from 2.4–1.5 GPa) and slight cooling (540–500 °C).

The second group of metapelite was identified only in the basement (Muret Unit). In these samples, coesite is absent and polycyclic garnet crystals are present. A narrow Alpine garnet rim overgrew pre-Alpine garnet relicts at much lower P (~2.1–2.2 GPa) than the quartz–coesite equilibrium. The absence of garnet growth at ultrahigh pressure (UHP) conditions in the second group of metapelite may be related to the details of the reaction mechanisms, especially the timing and amount of fluid access inside the system, as well as the consequent changing scale of the effective bulk compositions during garnet growth. In the polycyclic rocks, kinetics plays a major role.

We performed a review of garnet compositions in metapelites from a variety of terrains and P – T conditions, and we modelled the bulk-rock composition of an average metapelite. This shows (i) systematic variations of garnet composition with P – T conditions (decreasing grossular content with increasing P and increasing pyrope content with increasing T) and (ii) that the garnet compositions reported from the studied area are consistent with those described in other terrains equilibrated at the quartz–coesite transition.

1 Introduction

Coesite is an iconic mineral of the ultrahigh pressure (UHP) metamorphism (Chopin, 1984; Smith, 1984; Okay et al., 1989; Reinecke, 1991; Coleman and Wang, 1995; Wain, 1997; Compagnoni and Rolfo, 2003). Identification of coesite in metamorphic rocks relies on its optical properties (higher relief, lower birefringence compared to quartz); textural features (palisade texture, curved and radial microcracks around the inclusion), associated with its partial replacement by quartz during decompression; and Raman characterization of relict grains (Sharma et al., 1981; Boyer et al., 1985; Hemley, 1987; Gillet et al., 1990; Černok et al., 2014). Raman microspectroscopy has been shown to be of great help for detecting small, pristine inclusions of coesite (Korsakov et al., 2007; Taguchi et al., 2021; Manzotti et al., 2022; Ghignone et al., 2023, 2024). If the characterization of the (U)HP metamorphism is based solely on the occurrence of coesite, one may miss a large number of occurrences, because (i) some rocks may lack quartz (or coesite) during their entire metamorphic history, and (ii) small inclusions in garnet may escape even an expert petrographic examination of thin sections or require a large amount of patient work to be detected with the Raman micro-spectrometer. Therefore, another approach to detect UHP metamorphism, whether the studied rocks contain coesite crystals or not, is through thermodynamic modelling of coexisting minerals, especially garnet.

In the northern Dora-Maira Massif, coesite has been found in garnet-chloritoid micaschists from the Chasteiran Unit (Manzotti et al., 2022) that defines a small layer at the base of a polycyclic unit, locally named Muret Unit (Nosenzo et al., 2024). This paper investigates in detail the Alpine history of the Muret Unit and the overlying Serre Unit. Unexpectedly, thermodynamic P – T modelling suggested that the micaschists from these units also crystallized in the coesite stability field, on the basis of garnet chemistry. This prompted a careful Raman study, leading to the discovery of new coesite occurrences in garnet, which must have grown at or close to the quartz–coesite transition.

The above data are used for a careful discussion about equilibrium vs. kinetics of metamorphic reactions in the studied metapelites. Peak P – T conditions are modelled in the frame of the equilibrium paradigm (e.g., Powell and Holland, 2010; Anderson, 2017; Groppo, 2025, and references therein). However, recent studies have discussed the role of potential departures from equilibrium growth. These departures may be due to (i) restrictions or changes about the scale of equilibrium volumes and therefore the effective bulk composition used in the modelling (e.g., Yang and Rivers, 2001; Lanari and Engi, 2017; Evans et al., 2025), (ii) lack of fluid availability during part of the P – T path (Ridley and Thompson, 1986; Rubie, 1986), and (iii) overstepping of metamorphic reactions (Pattison et al., 2011; Carlson et al., 2015; Spear and Pattison, 2017; Evans et al., 2025).

2 Geological setting

The Dora-Maira Massif is located in the internal zone of the Western Alps (Bousquet et al., 2012), where it occurs as a large antiformal window below the eclogite-facies oceanic units (Ballèvre et al., 2020; Michard et al., 2022). The internal structure of the Dora-Maira Massif is characterized by the stacking of thin slices (Chopin et al., 1991; Henry et al., 1993; Groppo et al., 2019, 2025; Michard et al., 2022), essentially belonging to three main units (Figs. 1 and 2).

1. At the base, the lowermost unit (Sanfront-Pinerolo Unit) is characterized by graphite-rich meta-conglomerates, meta-sandstones, and a few former coal (now graphite; Santoro et al., 2025) layers that are assumed to be derived from Carboniferous sedimentary protoliths (Novarese, 1898; Petroccia and Iaccarino, 2022; Nosenzo et al., 2024), in accordance with the ages obtained through detrital zircon geochronology (Manzotti et al., 2016). A number of Permian-aged dioritic to granitic plutons intrude the sediments, dated using U-Pb geochronology on zircons (Bussy and Cadoppi, 1996). The metamorphic grade of the Sanfront-Pinerolo Unit is considered high-grade blueschist to eclogite facies, with P – T estimates of 2.0–2.4 GPa and 500–520 °C (Groppo et al., 2019).
2. The main body of the Dora-Maira Massif is made of units deriving from a polycyclic basement (e.g., Brossasco-Isasca Unit: Compagnoni and Rolfo, 2003; Muret Unit: Nosenzo et al., 2022, 2024). Polycyclism is best recorded by (i) granitic intrusions of Ordovician age (Bussy and Cadoppi, 1996; Nosenzo et al., 2024) and (ii) garnet relicts and staurolite pseudomorphs, an assemblage whose P – T conditions (\sim 0.6–0.7 GPa, \sim 650 °C) and age (\sim 325 Ma) have been defined using thermodynamic modelling and U-Pb geochronology on monazite, respectively (Nosenzo et al., 2022).
3. On top of these polycyclic units, thin slices are essentially made of felsic orthogneisses, monocyclic garnet-chloritoid micaschists, and dolomitic marbles and calc-schists (i.e. the Serre Unit, Manzotti et al., 2022; Nosenzo et al., 2024). The latter are considered to represent the parautochthonous Mesozoic cover of the Palaeozoic basement. The metamorphic grade of these units has not been studied in detail so far and will be explored in more detail in this paper.

Following our mapping work in a large sector between the Germanasca and Chisone valleys (Nosenzo et al., 2024), we are in possession of a few hundred samples, out of which we made more than 200 thin sections. In the Muret Unit and Serre Unit, we have selected a few samples of garnet-bearing micaschists, and we have proceeded to an extensive microchemical investigation, followed by thermodynamic modelling of their mineral assemblages. Because most of them

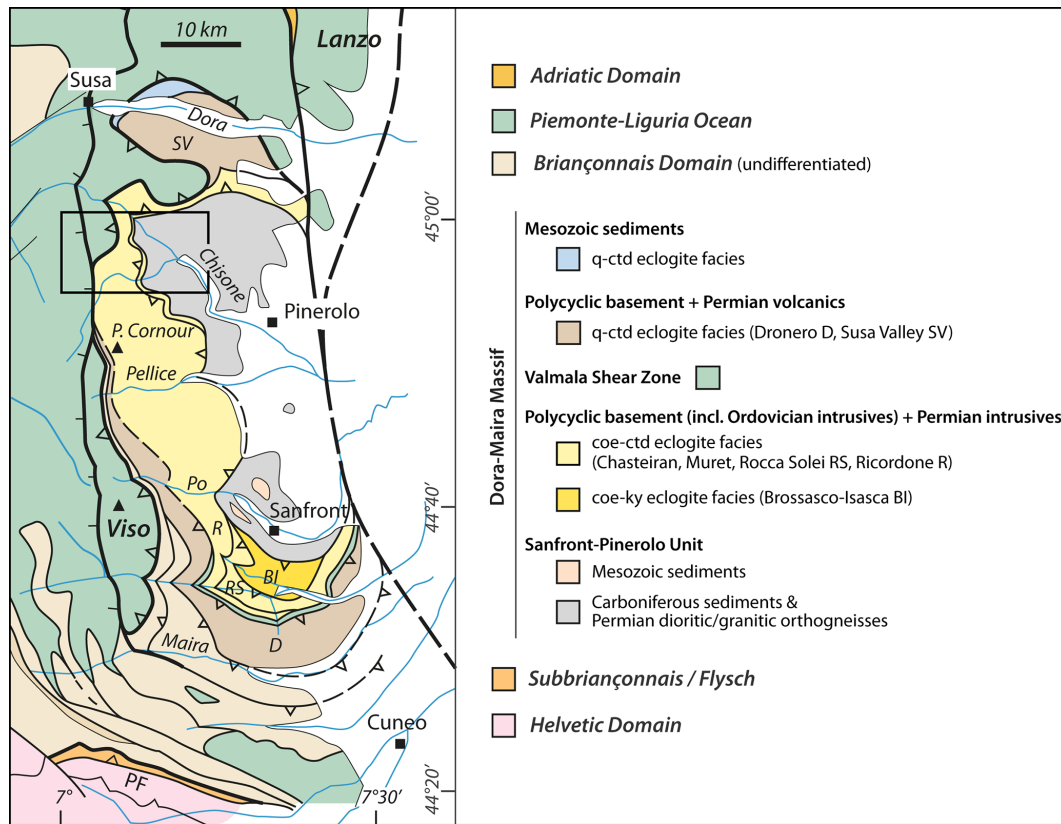


Figure 1. Structural setting of the Dora-Maira Massif (modified from Manzotti et al., 2025). The black rectangle indicates the location of the geological map of Fig. 2.

indicated equilibration of garnet in the coesite stability field, we proceeded to an extensive search for coesite by Raman micro-spectrometry, and indeed we found it in widely separated samples, belonging to the Muret Unit as well as to the Serre Unit (Fig. 2). This paper is therefore devoted to the petrological description of these samples.

3 Methods

3.1 Petrography, mineralogy, and whole-rock geochemistry

Hereafter, figures, tables, and sections given in the Supplement are referred to as “Fig. S”, “Table S”, and “Section S”. Samples were investigated by optical petrography and scanning electron microscopy in polished thin sections. Quantitative analyses of garnet and muscovite and X-ray compositional maps of garnet were acquired using an electron microprobe. Details on the operating conditions are given in Table S1. Mineral abbreviations are those used by THERMOCALC (Holland and Powell, 1998; Table S2), along with a list of other symbols used in this study. Because there is no formal definition of phengite and because there is no miscibility gap between muscovite and celadonite, muscovite is

used for potassic white mica, whatever its Si content. Representative analyses of selected minerals are given in Tables S3, S4, and S5.

The major element composition of three samples (MU23, MU7, and SE8; Table S6) collected in the Muret Unit and Serre Unit and used for phase diagram calculations was measured by X-ray fluorescence (XRF) at the PetroTectonic analytical facility at Stockholm University. Details about the method used for the analyses are available in Nosenzo et al. (2024).

3.2 Raman characterization of coesite

Given the relatively large number of garnet porphyroblasts ($40 < n < 86$) present in each thin section, a preliminary optical petrographic study was conducted in order to select the most promising garnet crystals (i.e. the ones with quartz/coesite inclusions). The number of selected garnet crystals for each sample varies from 3 to 12. Coesite inclusions in garnet were identified at the Laboratoire Magmas et Volcans (Clermont-Ferrand, France) using a Renishaw inVia confocal Raman micro-spectrometer equipped with a 532 nm diode-pulsed solid state laser, a Rayleigh rejection edge filter, a CCD detector of 1040×256 pixels, and a Leica DM 2500M

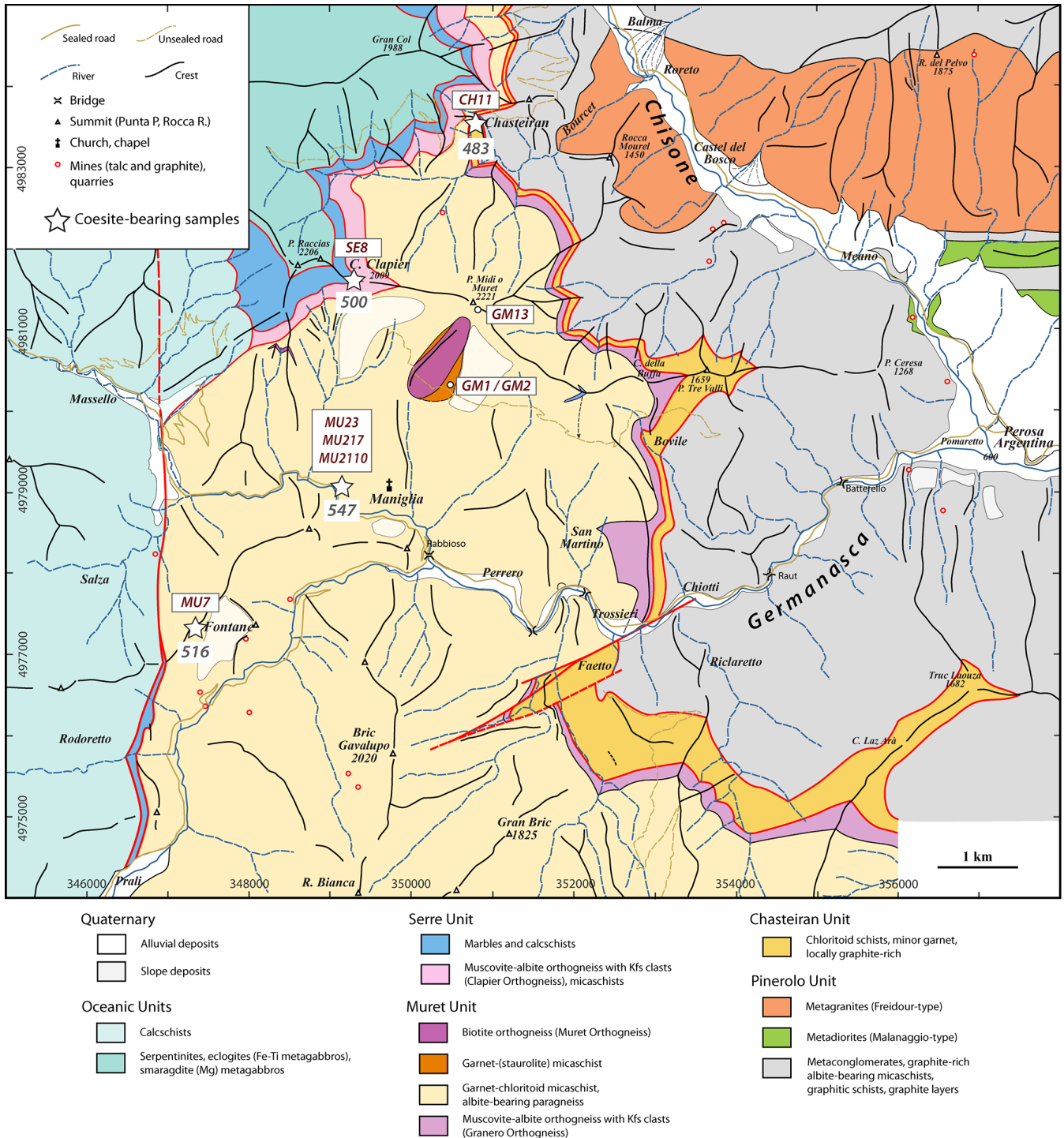


Figure 2. Structural setting of the studied area and sample location (modified from Nosenzo et al., 2024). *T* (°C) data estimated in this study and in Manzotti et al. (2022) by Raman spectroscopy on carbonaceous material (RSCM) are also reported (numbers in italic).

optical microscope with a motorized XYZ stage. The analyses were carried out in back-scattered geometry using a grating of 2400 grooves mm⁻¹, a 20 μm slit aperture (high focality setting), a 100× microscope objective, and ~7 mW laser power on the sample. These analytical conditions result

in a spatial lateral resolution of ~1 μm and vertical resolution of ~2–3 μm at the sample surface, as well as a spectral resolution of 0.4 cm⁻¹. Each analysis lasted 30 s (i.e., two accumulations of 15 s). Two-dimensional Raman mapping was performed with ~15 mW laser power on the sample, a spac-

ing of 0.5 μm , and exposure time of 5 s per point. Daily calibration of the spectrometer was performed by measuring the position of neon lines and the main peak of a silicon standard (520.5 cm^{-1}). A euhedral crystal of α -quartz manufactured by the company SICN (now Gemma Quartz and Crystal, Annecy, France) was used as standard to check analytical reproducibility during the analytical session (Table S7). Room temperature was maintained at 21 ± 1 °C. The spectra were acquired in the wavenumber range of ~ 90 – 1350 cm^{-1} and also in the O–H spectral region of ~ 3000 – 3800 cm^{-1} if a hydrous mineral was identified. After the analysis, fitting of the peaks of quartz (Table S7), coesite, and host garnet was performed using WiRE™ 4.4 software.

3.3 Thermodynamic modelling

Thermodynamic modelling was performed in order to produce isochemical phase diagrams, appropriate for depicting mineral assemblages for a given bulk composition (Powell and Holland, 1990, 2010). We have used the same approach as adopted in Manzotti et al. (2022), allowing for comparison with another sample from the northern Dora-Maira Massif (i.e. CH11, a coesite–chloritoid–garnet micaschist from the Chasteiran Unit). In detail, the modelling strategy was the following:

- Isochemical phase diagrams (i.e. pseudosections) were calculated with the Theriak/Domino software (de Capitani and Brown, 1987; de Capitani and Petrakakis, 2010), using the internally consistent thermodynamic data set 6.2 (Holland and Powell, 2011) and the suitable mixing models for solid solutions (converted for Theriak/Domino by D. K. Tinkham, <http://dtinkham.net/peq.html>, last access: 1 June 2018). The phases considered in the calculations, and the activity–composition models are given in Table S8.
- P – T phase diagrams were calculated in the chemical system MnO – Na_2O – CaO – K_2O – FeO – MgO – Al_2O_3 – SiO_2 – H_2O – TiO_2 – Fe_2O_3 (MnNCKFMASHTO) in the P – T ranges 1.5–3.5 GPa and 400–600 °C and 1.5–3.0 GPa and 450–600 °C.
- Given the negligible amount of Fe^{3+} in garnet, the limited modal amount of epidote, and the absence of Fe^{3+} -rich oxides (hematite and magnetite), the amount of Fe^{3+} was set to 5 % of total Fe [$X(\text{Fe}^{3+}) = \text{Fe}^{3+} / \text{Fe}_{\text{total}}$] (see also Manzotti et al., 2018, and Manzotti et al., 2024, for details on this assumption).
- The fluid phase was fixed as pure H_2O . Given the P – T conditions of interest, this assumption is valid despite the local presence of graphite (Connolly and Cesare, 1993).

- The effects of fractionation of the zoned garnet (e.g. Tinkham and Ghent, 2005; Zuluaga et al., 2005) were considered. In order to model the growth of the garnet outer core, a second pseudosection was calculated by subtracting the composition of the garnet inner core from the measured bulk composition. Similarly, to estimate the P – T conditions corresponding to the growth of the garnet rim, a third pseudosection was calculated by subtracting the composition of both the garnet inner and outer core from the measured bulk composition. Details on garnet fractionation are given in Sect. S1.
- Because decompression may lead to H_2O undersaturation (following Guiraud et al., 2001), one pseudosection was calculated in the P – T range 1.5–3.0 GPa and 400–600 °C with a fixed amount of H_2O (following Le Bayon et al., 2006; Manzotti et al., 2018, 2022; Nosenzo et al., 2023; Manzotti et al., 2025). This amount was determined so that the proportion of the fluid phase in the rock does not exceed 1 vol % (Thompson and Connolly, 1990) at peak T (inferred from Fig. 4b for sample MU23 and from Fig. 9b for sample SE8).

Finally, Raman spectroscopy on carbonaceous material (RSCM; Beyssac et al., 2002) was also applied to estimate the maximum T registered by the studied samples (details on the method are given in Sect. S2). This method provides an estimation of maximum T , which is independent of the equilibrium thermodynamics approach used by Theriak/Domino.

4 Thermodynamic modelling of the coesite-bearing samples

4.1 Garnet–glaucofane micaschist from the Muret Unit (MU23, MU217, MU2110)

A set of samples have been collected along the road close to Maniglia (lat/long coordinates 44°56′54.10″ N, 7°05′13.15″ E; Fig. 2). Amongst these samples, there are slight differences: most of them are garnet–glaucofane quartz-rich micaschists, displaying only a few chloritoid crystals in the matrix (samples MU23 and MU217, Figs. S1–6), whereas a few of them are characterized by a larger proportion of matrix chloritoid and minor amount of glaucofane crystals (sample MU2110, Figs. S7–8). In addition, some samples display only one well-developed foliation (e.g., Figs. S1–4), whereas in others the main foliation is overprinted by small-scale crenulation folds (Figs. S5–6).

In sample MU23, the foliation is defined by the shape-preferred orientation of white mica, mainly consisting of paragonite with minor muscovite. The latter displays chemical zoning, with decreasing Si content and X_{Mg} and increasing X_{Na} from core (Si = 3.48–3.51 a.p.f.u. (atoms per formula unit); $X_{\text{Mg}} = 0.77$ – 0.80 ; $X_{\text{Na}} = 0.01$ – 0.02) to rim (Si = 3.23–3.38 a.p.f.u.; $X_{\text{Mg}} = 0.52$ – 0.69 ; $X_{\text{Na}} = 0.04$ – 0.06). Garnet occurs as idioblastic to sub-rounded crystals

(up to 4 mm in size) wrapped by the main foliation (Figs. S1–8). Inclusions of rutile, chloritoid, white mica, quartz/coesite (see below), and accessory minerals (mainly zircon) are common (Fig. 3a). Lozenge-shaped domains (up to 1 cm long) are interpreted as glaucophane pseudomorphs (e.g., Figs. S1–4). Detailed SEM studies of these domains indicate that the submicroscopic aggregates replacing glaucophane consist of albite, green amphibole, chlorite, pale brown-green biotite, and minor quartz. Pseudomorphs locally display small garnet inclusions (up to 200 μm in size) and overgrow the larger garnet porphyroblasts (Figs. S1 and S3). Chlorite in the matrix occurs in minor modal amount, as crystals oriented either parallel to the main foliation or at moderate to high angle with respect to this fabric. Ilmenite is the main Ti-bearing oxide in the matrix and replaces rutile.

4.1.1 Garnet chemistry

Garnet crystals in sample MU23 show chemical and microstructural features similar to the garnets described by Manzotti et al. (2022) in the UHP Chasteiran micaschists (Fig. 3). Specifically, garnet porphyroblasts display two stages of growth that correspond to cores (by far the largest part of garnet grains) and rims (about 200 μm thick), respectively. Both are characterized by distinct and characteristic zoning patterns, but they are not separated by an optical discontinuity.

Spessartine decreases (spss from 6 mol %–2 mol %) continuously from the centre of the inner cores to the edge of the outer cores, whereas almandine remains almost constant (alm \sim 79 mol %–80 mol %) and slightly decreases (from 80 mol %–78 mol %) only in the outermost cores. The grossular (grs \sim 6 mol %–7 mol %) and pyrope (prp \sim 6 mol %) contents remain approximately constant over the inner cores and most of the outer cores and increase at the outermost cores (grs up to \sim 12 mol %; prp up to 13 mol %). Garnet rims show a sharp increase in grossular (from 12 mol %–20 mol %) and a decrease in pyrope (from 13 to 3 mol %) and spessartine (from 2 mol %–1 mol %, Fig. 3b). Almandine slightly increases (from 78 mol %–83 mol %) and then slightly decreases (from 83 mol %–79 mol %).

4.1.2 P – T conditions for garnet growth

To model the growth of the *garnet inner cores*, a phase diagram was calculated in the system MnNCKFMASHTO using the whole-rock bulk composition and H_2O in excess. Comparison between the measured garnet inner core composition (spss = 6 mol %, grs = 6–7 mol %) and the corresponding isopleths indicates that the growth of garnet inner cores initiated in the g-ctd-jd-gl-law-mu-q-ru field, just below the coesite–quartz transition, at \sim 2.6–2.7 GPa and \sim 510–530 $^{\circ}\text{C}$. We note that the modelled content of pyrope (prp = 9 mol %) is slightly higher than the one measured (prp = 6 mol %).

A second phase diagram was calculated in the same P – T range (1.5–3.5 GPa, 400–600 $^{\circ}\text{C}$) considering garnet fractionation (see Sects. 3.3 and S1 for details) with the aim to determine the P – T conditions for the *garnet outer cores*. Garnet fractionation does not change the main topology of the phase diagram, but mainly displaces the garnet-in line at higher T by \sim 20 $^{\circ}\text{C}$. The zoning of the garnet outer cores is compatible with its growth (\sim 3 vol %) along a prograde up-pressure up-temperature P – T trajectory: it is almost subparallel to the grossular isopleths (grey arrow in Fig. 4a) and reaches the coesite stability field at 2.7–2.9 GPa and 530–550 $^{\circ}\text{C}$. The outermost part of garnet cores shows an increase in pyrope (6 mol %–13 mol %) and grossular (6 mol %–12 mol %). This is compatible with the growth of the outermost part of the garnet cores (\sim 0.5 vol %) along a P – T path characterized by a nearly isothermal decompression (from 2.9 to 2.4 GPa). The Si content of muscovite modelled at peak P – T conditions (3.40–3.45 a.p.f.u.) is slightly lower than the Si content (3.48–3.51 a.p.f.u.) measured in the core of the muscovite marking the S_{1-2} foliation, but it is nevertheless compatible with growth during the end of the burial.

To model the growth of *garnet rims*, a phase diagram was calculated in the P – T range 1.5–3.0 GPa and 400–600 $^{\circ}\text{C}$, with a fixed amount of H_2O and considering garnet fractionation (see Sects. 3.3 and S1 for details). Despite the restrictive condition with respect to the H_2O availability, the major portion of the phase diagram shows fluid-present assemblages (Fig. 5a). The zoning of the garnet rims, characterized by a strong increase in grossular (12 mol %–20 mol %) and by a decrease in pyrope (13 mol %–3 mol %), indicates its growth during decompression (from \sim 2.4 to \sim 1.6 GPa) and slight cooling (from \sim 550 to 530 $^{\circ}\text{C}$) in the lawsonite-absent domain (Fig. 5b). Comparison between modelled and measured (Si = 3.23–3.38 a.p.f.u.) Si content in muscovite suggests that the growth of muscovite rims occurred during decompression along the P – T path inferred from the zoning of the garnet rims.

4.2 Garnet-chloritoid micaschist from the Muret Unit (MU7)

Sample MU7 has been collected close to Fontane (lat/long coordinates 44 $^{\circ}$ 56'05.10" N, 7 $^{\circ}$ 04'10.18" E; Fig. 2). This foliated garnet-chloritoid micaschist (Figs. S9–11) displays quartz-rich lenses alternating with mica-rich layers. Chloritoid is frequently densely packed in micro-domains that are thicker than the quartz- and muscovite-rich layers (Fig. S11). The foliation has a complex history, as recorded by (i) intrafolial isoclinal folds deforming an S_1 foliation, (ii) a main fabric (S_2) parallel to the quartz and mica layers and wrapping the chloritoid-rich domains, and (iii) a few shear bands cutting across the S_2 foliation. The mica layers marking the S_{1-2} foliation mainly consist of muscovite which displays chemical zoning, with decreasing Si con-

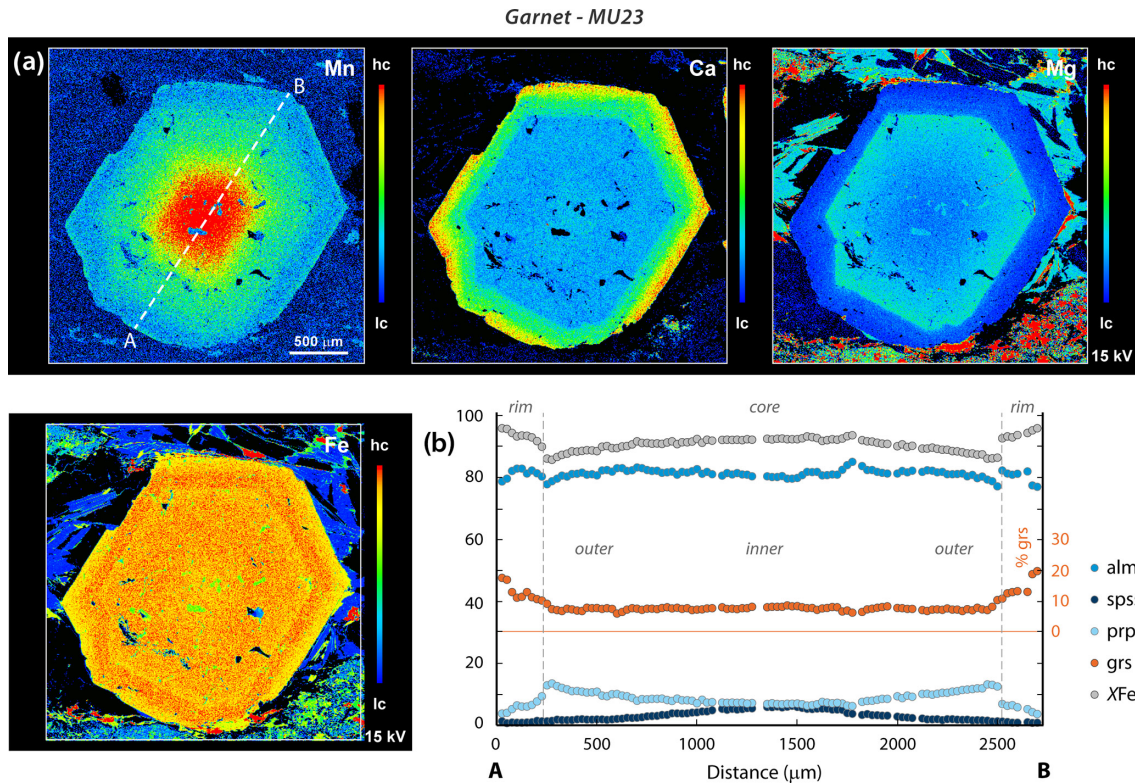


Figure 3. (a) X-ray maps of a garnet from sample MU23. The interface between garnet core and rim is quite regular. (b) Compositional profile of garnet for sample MU23. The position of the profile (line A–B) is reported on the X-ray map of Mn.

tent and X_{Mg} and increasing X_{Na} from core ($Si = 3.40$ – 3.51 a.p.f.u.; $X_{Mg} = 0.68$ – 0.75 ; $X_{Na} = 0.01$ – 0.03) to rim ($Si = 3.29$ – 3.37 a.p.f.u.; $X_{Mg} = 0.55$ – 0.75 ; $X_{Na} = 0.04$ – 0.08).

Garnet crystals (up to 1 mm in size) are dispersed throughout the rock, with the exception of the chloritoid-rich domains (Figs. S9–11). Their shape varies from idioblastic to sub-rounded. Most of them display tiny inclusions of rutile, quartz-coesite (see below), muscovite, and accessory minerals: inclusions do not define an internal foliation (Fig. 6a). Garnet crystals are frequently partially replaced by chlorite at the rims and along fractures. Glaucophane pseudomorphs (up to 1 cm long, Fig. S10) consist of very fine-grained aggregates of albite and chlorite and are dispersed in the rock. The pseudomorphs retain the original shape of the glaucophane crystals, which were aligned along the S_{1-2} foliation, suggesting that the replacement reactions took place after the end of pervasive ductile deformation.

Matrix rutile grains (up to $100\ \mu\text{m}$ in size) are aligned parallel to the S_{1-2} foliation and are partially or completely replaced by ilmenite. By contrast, rutile inclusions in garnet and chloritoid are devoid of ilmenite corona.

4.2.1 Garnet chemistry

Garnet crystals display one stage of growth and no evidence of polycyclism (Fig. 6). Their major element zoning

pattern is similar to the one shown by the garnet cores of sample MU23. The second stage of growth corresponding to the Ca-rich rims is only barely represented. Garnet cores show a continuous decrease in spessartine (from 11 mol %–2 mol %) and an increase (from 77 mol %–81 mol %) in almandine from the centre of the cores to the edge of the outer cores (Fig. 6b). Locally, almandine slightly decreases (from 81 mol %–79 mol %) in the outermost cores. The grossular and pyrope contents remain approximately constant over the inner cores and increase only in correspondence of the thin (from ~ 50 to $\sim 100\ \mu\text{m}$) outermost cores (grs: 5 mol %–9 mol %; prp: 5 mol %–10 mol %).

4.2.2 P – T conditions for garnet growth

As for sample MU23, to model the growth of the garnet inner cores, a phase diagram was calculated using the whole-rock bulk composition and H_2O in excess. Comparison between the measured garnet inner core composition (spss = 11 mol %, grs = 5 mol %–6 mol %) and the corresponding isopleths indicates that crystallization of the garnet inner cores (~ 2 vol %) initiated at ~ 2.7 – 2.8 and ~ 500 – $530\ ^\circ\text{C}$ at the quartz–coesite transition (Fig. 7a and c). As for sample MU23, we note that the modelled pyrope content (prp = 7 mol %) is slightly higher than the one measured (prp = 5–6 mol %).

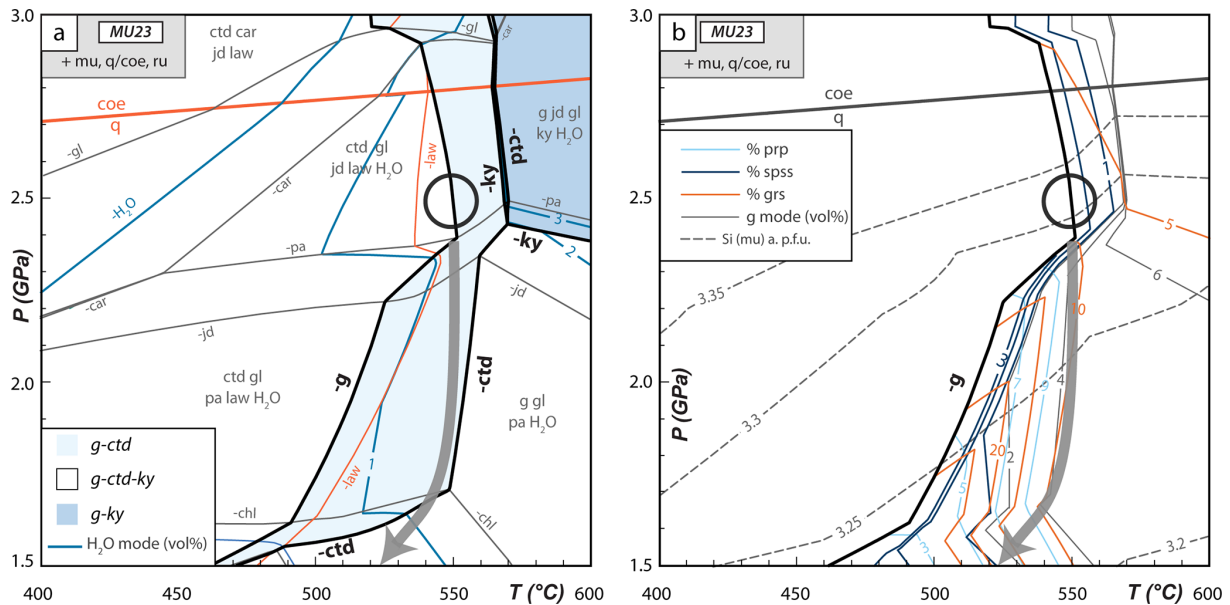


Figure 5. P – T phase diagrams calculated for sample MU23, considering progressive garnet fractionation. **(a)** P – T phase diagram calculated in the range 15–30 kbar and 400–600 °C, using the bulk-rock composition obtained by garnet core (inner and outer core) fractionation and using a fixed amount of H_2O . The H_2O modal amount is also shown. The pale blue area represents the stability field of the garnet- and chloritoid-bearing assemblages. The dark blue domain indicates the stability field of garnet- and kyanite-bearing assemblages. The lower variance garnet–chloritoid–kyanite assemblage is stable in an intermediate, very narrow (in T), domain (left in white for the sake of clarity). **(b)** Chemical and modal isopleths (garnet and muscovite) calculated for **(a)**. The grey arrow in **(a)** and **(b)** is the inferred P – T path followed during the growth of garnet rim.

tween modelled and measured Si contents in muscovite suggests that the cores of this mineral (Si = 3.40–3.51 a.p.f.u.) grew at P – T conditions similar to the ones of garnet inner cores (Fig. 6c). By contrast, muscovite rims (Si = 3.29–3.37 a.p.f.u.) crystallized during the nearly isothermal decompression (Fig. 6d).

4.3 Garnet-chloritoid micaschist from the Serre Unit (SE8)

Sample SE8 was collected close to the Col Clapier in the Serre Unit (lat/long coordinates 44°58′19.67″ N, 7°05′14.83″ E; Fig. 2). It is a foliated garnet-chloritoid micaschist and displays microstructural features similar to sample MU7. Quartz-rich lenses alternate with mica-rich layers, whereas chloritoid is densely packed in micro-domains that are thicker than the quartz- and muscovite-rich layers (Figs. S12–17). Intrafolial isoclinal folds deform an S_1 foliation, while the main fabric (S_2) is parallel to the quartz and mica layers and wraps the chloritoid-rich domains. A few shear bands cut across the S_2 foliation (Fig. S12). Muscovite, defining the S_{1-2} foliation, displays chemical zoning, with decreasing Si content and X_{Mg} and increasing X_{Na} from core (Si = 3.42–3.50 a.p.f.u.; X_{Mg} = 0.72–0.78; X_{Na} = 0.01–0.04) to rim (Si = 3.23–3.35 a.p.f.u.; X_{Mg} = 0.55–0.76; X_{Na} = 0.05–0.07).

Idioblastic to sub-rounded garnet crystals (up to 1 mm in size) are dispersed throughout the rock, with the exception of the chloritoid-rich domains (Figs. S12–17). Most of them contain tiny inclusions of rutile, quartz-coesite (see below), muscovite, and accessory minerals that do not define an internal foliation. Garnet crystals are frequently heavily replaced by chlorite at the rims and along fractures (Figs. 8a, S12, and S14). Rare glaucophane pseudomorphs (up to 0.5 cm long) consist of very fine-grained aggregates of albite and chlorite. The pseudomorphs retain the original shape of the glaucophane crystals, which were aligned along the S_{1-2} foliation, suggesting that the replacement reactions took place after the end of ductile deformation. Chlorite is quite abundant in the rock and statically replaces garnet. In addition, a few crystals are growing in the matrix without a preferred orientation suggesting that their growth postdates the main ductile deformation (Fig. S12). Matrix rutile grains (up to 100 μ m in size) are aligned parallel to the S_{1-2} foliation and are partially or completely replaced by ilmenite. By contrast, rutile inclusions in garnet and chloritoid are devoid of ilmenite corona.

4.3.1 Garnet chemistry

The chemistry and microstructure of garnet in sample SE8 are similar to those of garnet described in samples MU23 (Muret Unit, this study) and CH11 (Chasteiran Unit; Manzotti et al., 2022). Garnet crystals show two stages of growth

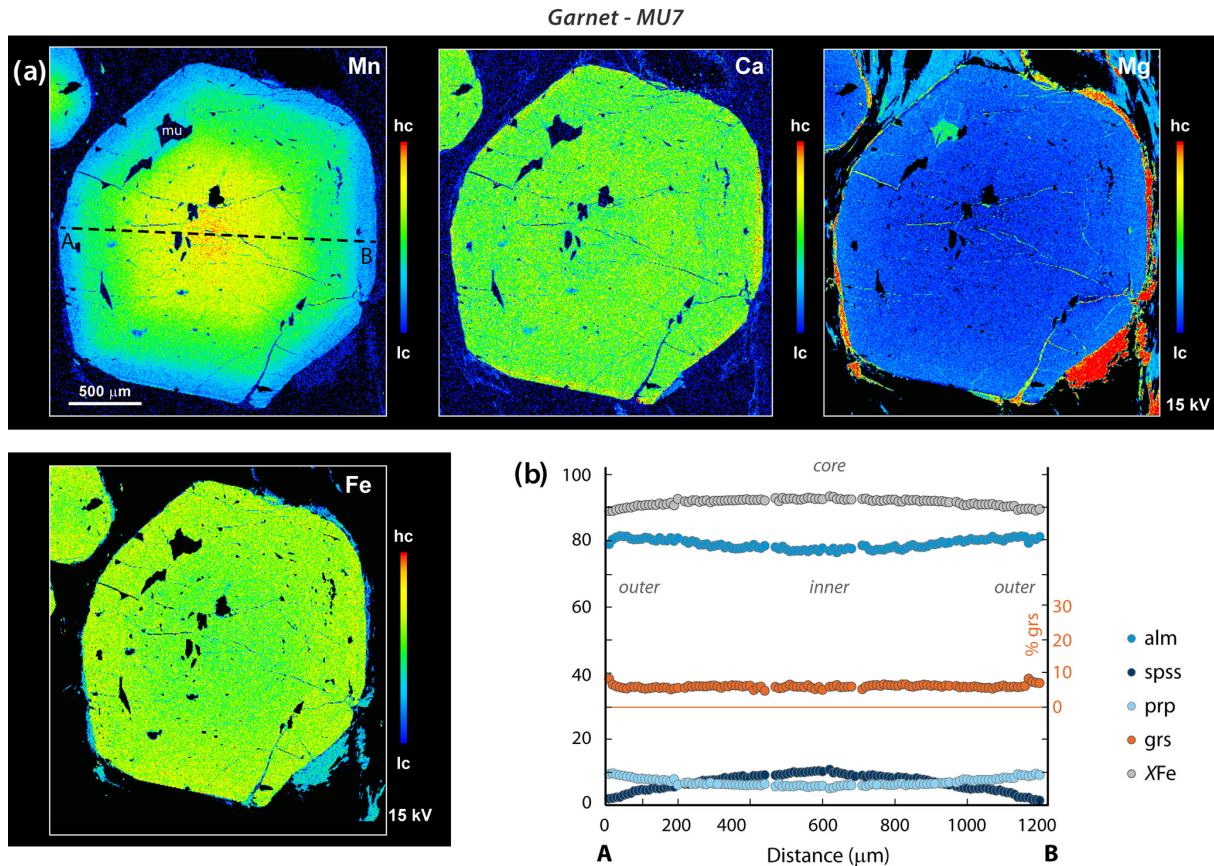


Figure 6. (a) X-ray maps of a garnet from sample MU7. Note the absence of the Ca-rich rim. (b) Compositional profile of garnet for sample MU7. The position of the profile (line A–B) is reported on the X-ray map of Mn.

(Fig. 8a): colourless cores and thin pink rims are only rarely separated by an optical discontinuity, but they can be distinguished on the basis of their zoning pattern.

Spessartine decreases (from 10 mol %–2 mol %) continuously from the centre of the inner cores to the edge of the outer cores, whereas almandine slightly increases (from 76 mol %–80 mol %). The grossular (grs ~ 5 mol %–6 mol %) contents remain approximately constant over the inner cores and most of the outer cores and increase at the outermost cores (grs up to ~ 10 mol %). Pyrope continuously increases from the inner cores to the outer cores (6 mol %–11 mol %). Garnet rims show a sharp increase in grossular (10 mol %–26 mol %) and a decrease in pyrope (10 mol %–3 mol %), spessartine (2 mol %–1 mol %), and almandine (80 mol %–75 mol %, Fig. 8b).

4.3.2 P – T conditions for garnet growth

As for samples MU23 and MU7, to model the growth of the *garnet inner cores*, a phase diagram was calculated in the system MnNCKFMASHTO using the whole-rock bulk composition and H₂O in excess. Comparison between the measured garnet inner cores composition (grs = 5–6 mol %,

prp 6 mol %) and the corresponding isopleths indicates that the growth of garnet inner cores started at ~ 2.5 GPa and ~ 470 °C (Fig. 9a and c). The modelled spessartine content in the correspondence of the onset of the inferred P – T path (spss = 30 mol %) is higher than the one measured (spss = 10 mol %), but then decreases with increasing T .

A second phase diagram was calculated in the same P – T range (1.5–3.5 GPa, 400–600 °C) considering garnet fractionation (see Sects. 3.3 and S1 for details) with the aim to determine the P – T conditions for *garnet outer cores*. The garnet chemistry is compatible with a prograde up-pressure up-temperature P – T path, which is almost sub-parallel to the grossular isopleths and crosses the quartz–coesite transition close to the peak P – T conditions (i.e. ~ 2.9 GPa and ~ 530 °C, garnet mode ~ 1.8 vol %; Fig. 9b and d). The outermost portion of the garnet outer cores displays an increase in pyrope (6 mol %–11 mol %) and grossular (5 mol %–9 mol %). This trend is compatible with its growth (~ 0.2 vol %) during a nearly isothermal decompression (from 2.9 to 2.4 GPa and 530–540 °C; Fig. 9d). Comparison between modelled and measured Si content in muscovite suggests that the cores of this mineral (Si = 3.42–3.50 a.p.f.u.) grew at P – T conditions similar to the ones of

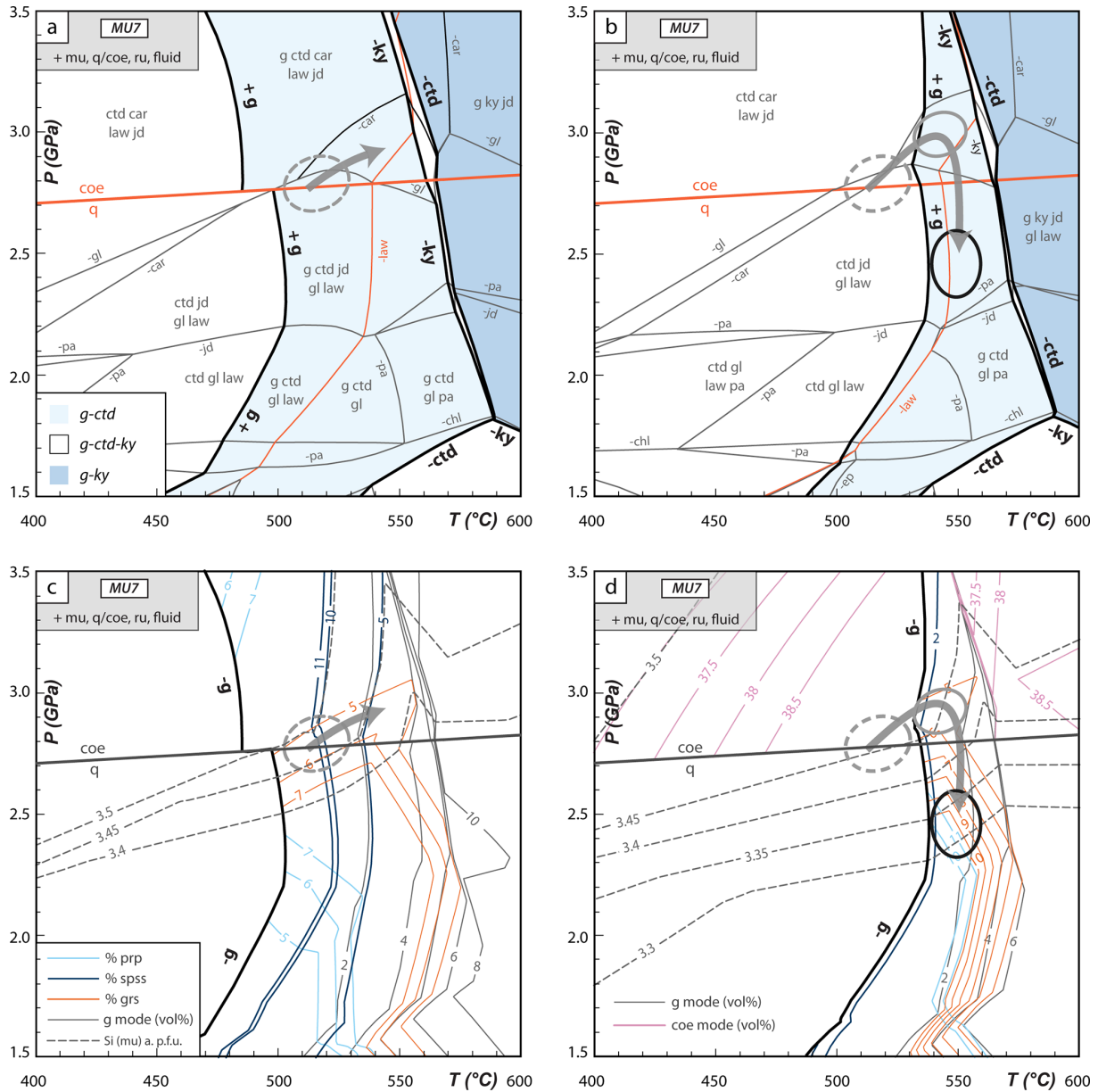


Figure 7. H₂O-saturated *P*–*T* phase diagrams calculated for sample MU7 using the unfractionated whole-rock composition (a) and a composition from which the garnet inner core has been subtracted (b). The pale blue area represents the stability field of the garnet- and chloritoid-bearing assemblages. The dark blue domain indicates the stability field of garnet- and kyanite-bearing assemblages. The lower variance garnet–chloritoid–kyanite assemblage is stable in an intermediate, very narrow (in *T*), domain (left in white for the sake of clarity). Some fields are not labelled for the sake of clarity; their assemblages can be deduced from the assemblages in the adjacent fields. *P*–*T* conditions for the growth of the garnet inner (dashed circle) and outer core (grey and black circles) are indicated. (c, d) Same *P*–*T* diagrams as above, displaying chemical and modal isopleths (garnet, muscovite, and coesite) calculated for (a) and/or (b).

garnet inner cores. By contrast, muscovite rims (Si = 3.23–3.35 a.p.f.u.) crystallized during the nearly isothermal decompression.

To model the growth of *garnet rims*, a phase diagram was calculated in the *P*–*T* range 1.5–3.0 GPa and 400–600 °C, with a fixed amount of H₂O and considering garnet fractionation (see Sects. 3.3 and S1 for details). As observed in

the case of sample MU23, despite the restrictive condition with respect to the H₂O availability, the major portion of the phase diagram shows fluid-present assemblages. Garnet rims display a strong increase in grossular (10 mol %–26 mol %) and a decrease in pyrope (10 mol %–3 mol %). This is compatible with its growth (~2.5 vol %) during decompression

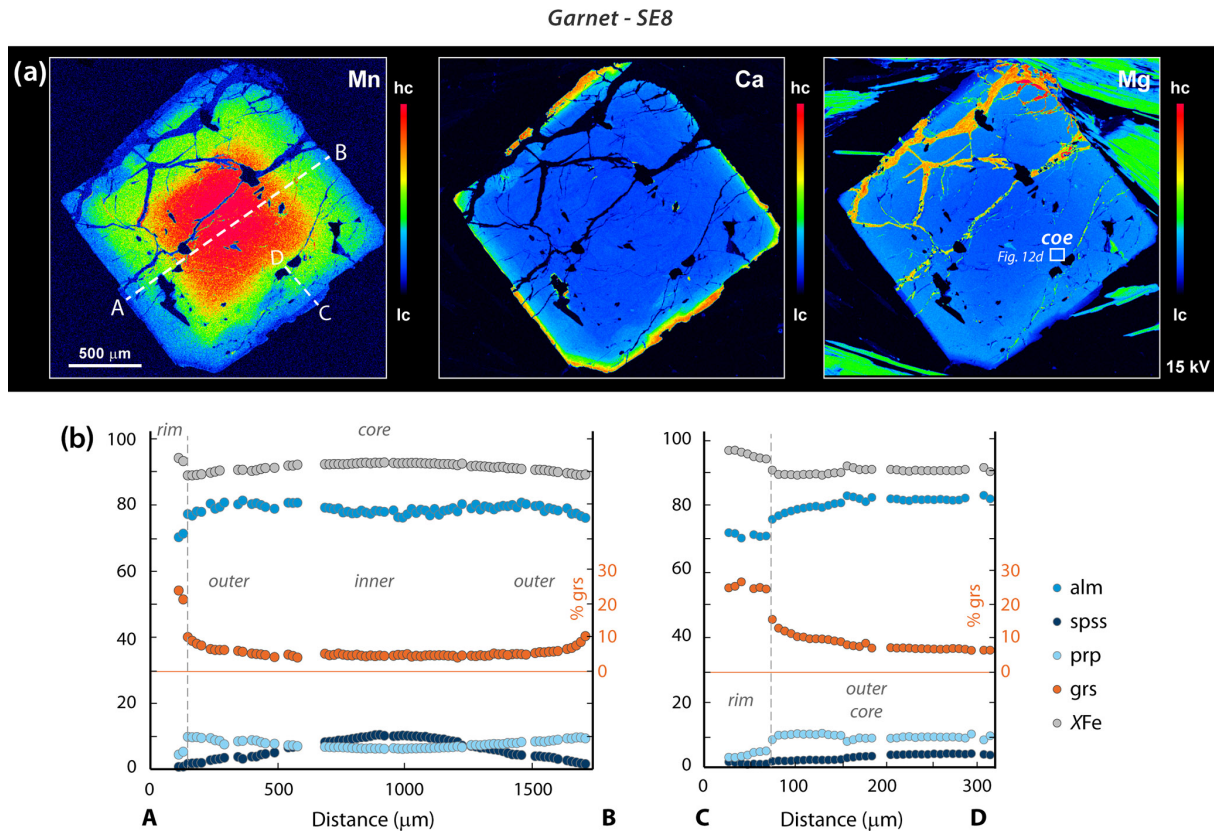


Figure 8. (a) X-ray maps of a garnet from sample SE8. Garnet displays a thin grossular-rich rim, partially dissolved and replaced by chlorite. The white square indicates a coesite inclusion (see Fig. 12d for a closer look). (b) Compositional profiles of garnet for sample MU23. The positions of the profiles (lines A–B and C–D) are reported on the X-ray map of Mn.

(from ~ 2.4 to ~ 1.5 GPa) and slight cooling (from ~ 540 to 520 °C), mainly in the lawsonite-absent domain (Fig. 10).

4.4 RSCM temperature

RSCM temperatures were estimated on samples collected both in the Muret Unit and Serre Unit (Fig. 2). Results are given in Table S9 and shown in Fig. 11. Because graphite is absent in samples MU23 and MU217 from the Maniglia locality, we used sample MU2110 from the same locality. In the latter sample, graphite yields consistent R^2 values, ranging from 0.16–0.29, with the exception of one crystal characterized by lower R^2 value (0.11). The average T for this sample is 547 ± 22 °C. Graphite in sample MU7 (Fontane locality, Muret Unit) yields rather consistent R^2 values in the range 0.20–0.34, with the exception of two crystals characterized by higher R^2 values (0.36 and 0.38). This sample displays a slightly lower T (average T of 516 ± 22 °C) than sample MU2110. In the Serre Unit, sample SE8 yields a RSCM T of 500 ± 48 °C. Most of the analysed graphite crystals yield R^2 values in the range 0.29–0.46, with a few crystals characterized by lower R^2 values, in the range 0.12–0.18. Overall, the three samples investigated in this study display

a maximum RSCM T of ~ 550 °C, which is compatible with the maximum T estimated with thermodynamic modelling. These values are slightly higher than the one measured in the Chasteiran micaschist (Fig. 11).

5 New coesite occurrences in the northern Dora-Maira Massif

Modelled P – T conditions in the three micaschist samples indicate that prograde garnet growth took place inside the coesite stability field or ended in the coesite stability field. Therefore, the search of coesite inclusions in garnet was conducted in five samples. Amongst them, coesite was identified in three samples collected in the Muret Unit (samples MU217 and MU7 from Maniglia and Fontane localities, respectively) and Serre Unit (sample SE8 from Col Clapier, Fig. 2).

Coesite occurs as tiny (from 10 to $50 \mu\text{m}$ in size) pristine inclusions a few micrometres below the surface of the thin section, in the centre as well as at the edge of the garnet cores (Fig. 12). By contrast, it is always absent in the grossular-rich garnet rims, as already noted in the coesite-bearing micaschist from the Chasteiran Unit (Manzotti et al.,

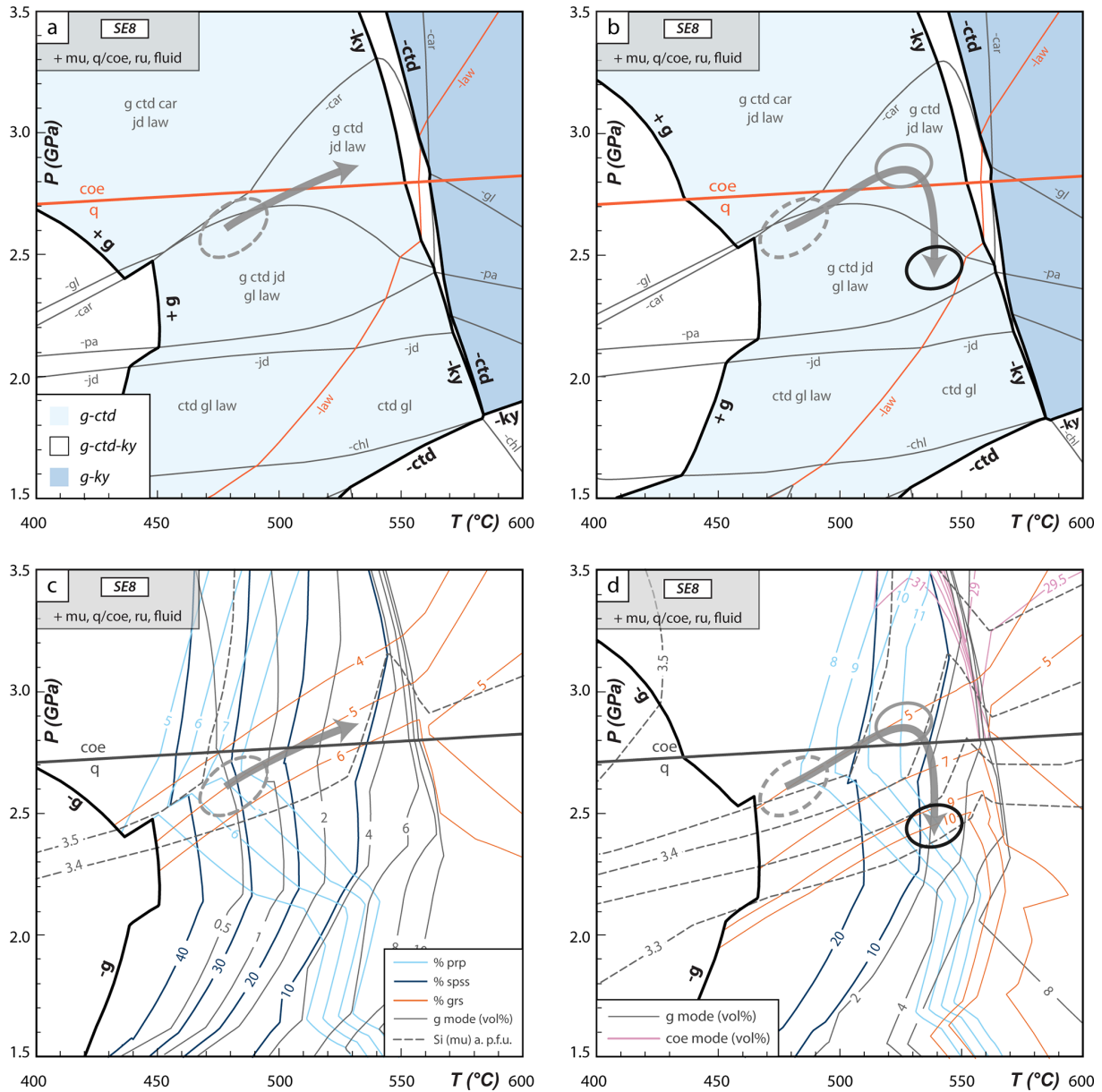


Figure 9. H₂O-saturated *P*–*T* phase diagrams calculated for sample MU23 using the unfractioanated whole-rock composition (a) and a composition from which the garnet inner core has been subtracted (b). The pale blue area represents the stability field of the garnet- and chloritoid-bearing assemblages. The dark blue domain indicates the stability field of garnet- and kyanite-bearing assemblages. The lower variance garnet–chloritoid–kyanite assemblage is stable in an intermediate, narrow (in *T*) domain (left in white for the sake of clarity). Some fields are not labelled for the sake of clarity; their assemblages can be deduced from the assemblages in the adjacent fields. *P*–*T* conditions for the growth of the garnet inner (dashed circle) and outer core (grey and black circles) are indicated. (c, d) Chemical and modal isopleths (garnet, muscovite, and coesite) calculated for (a) and/or (b) are shown.

2022). Some garnet porphyroblasts contain a single coesite inclusion (Figs. 8a and 12b); other ones display several ones (up to 5 grains identified in the same garnet crystal) generally distributed in different parts of the core (Fig. 12a and c). The shape of the crystals is quite variable, from ovoid to acicular (Fig. 13a–b). Some crystals show small embayments

and concave boundaries (Fig. 13b), other ones display a thin quartz corona as imaged by Raman mapping (Fig. 13a).

Included coesite displays the diagnostic Raman spectrum, characterized by more than 15 vibrational modes (e.g., Sharma et al., 1981; Boyer et al., 1985; Hemley 1987; Gillet et al., 1990; Černok et al., 2014) with the most intense band at 521 cm⁻¹. Some inclusions display a slight Raman shift

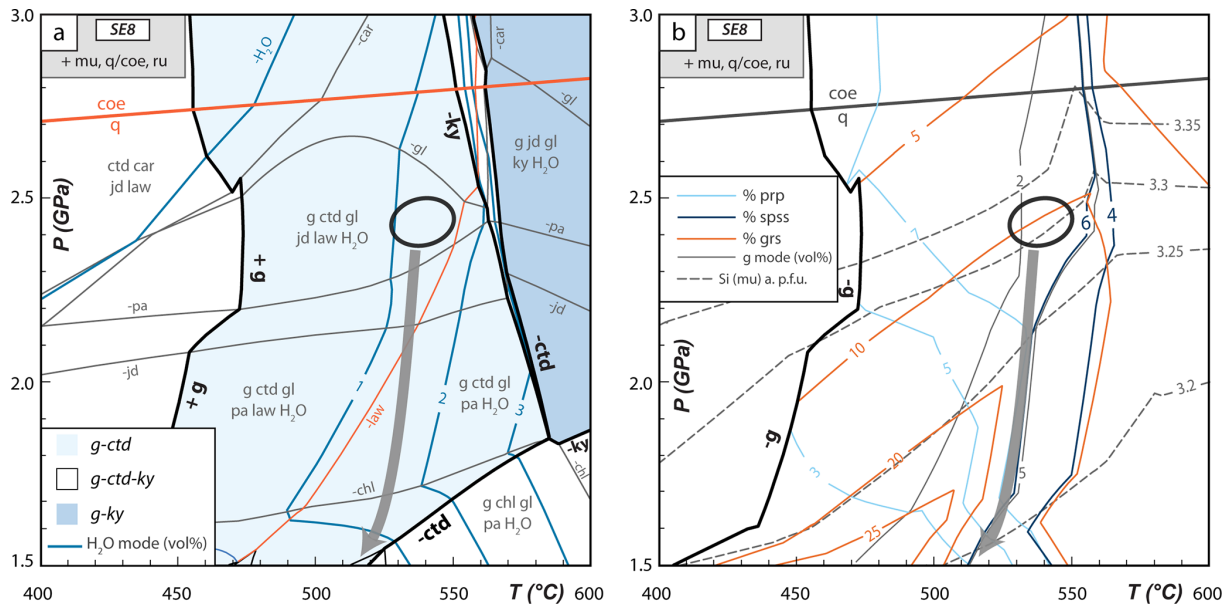


Figure 10. P – T phase diagrams calculated for sample SE8, considering progressive garnet fractionation. **(a)** P – T phase diagram calculated in the range 15–30 kbar and 400–600 °C, using the bulk-rock composition obtained by garnet core (inner and outer core) fractionation and a fixed amount of H_2O . The H_2O modal amount is also shown. The pale blue area represents the stability field of the garnet- and chloritoid-bearing assemblages. The dark blue domain indicates the stability field of garnet- and kyanite-bearing assemblages. The lower variance garnet–chloritoid–kyanite assemblage is stable in an intermediate, very narrow (in T), domain (left in white for the sake of clarity). **(b)** Chemical and modal isopleths (garnet and muscovite) calculated for **(a)**. The grey arrow in **(a)** and **(b)** is the inferred P – T path followed during the growth of garnet rim.

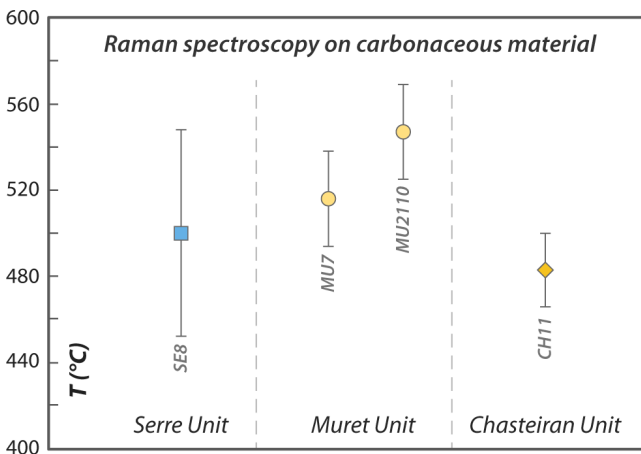


Figure 11. RSCM temperatures of the samples from the Muret Unit and Serre Unit. Data on sample CH11 are from Manzotti et al. (2022).

of its main coesite peak ($\nu = 522.5 \text{ cm}^{-1}$ sample MU7 and $\nu = 523.6 \text{ cm}^{-1}$ sample MU217, Fig. 13c). Some residual pressure is also recorded by the shift in the main Raman band of quartz measured in the quartz replacing coesite at the inclusion–host interface ($\nu = 465.9 \text{ cm}^{-1}$ sample MU217).

6 Discussion

Garnet–chloritoid micaschists, the most common lithology in the northern Dora-Maira Massif, may be divided into two principal categories. In the first one, we found evidence for one garnet generation (sample CH11 from the Chasteiran Unit (Manzotti et al., 2022, 2025) and, in this study, samples MU23, MU217, MU2110, and MU7 from the Muret Unit, as well as sample SE8 from the Serre Unit). In the second one, relicts of a pre-Alpine garnet are also observed (samples GM1, GM2, and GM13 from the Muret Unit; Nosenzo et al., 2022, 2023). Coesite has been identified in the samples from the first group (samples CH11, MU217, MU7, and SE8). By contrast, coesite has not been found so far in rocks from the Muret Unit displaying polycyclic garnet (see Nosenzo et al., 2022, 2023). A further difference between the coesite-bearing and the coesite-absent rocks is that garnet is (i) nucleating close to and growing across the quartz–coesite boundary in the coesite-bearing samples and (ii) overgrowing as narrow rim pre-Alpine garnets at much lower P (~ 2.1 – 2.2 GPa; Nosenzo et al., 2023) than the quartz–coesite equilibrium. Potential explanations for this first-order difference are the following.

1. A first explanation could be that the so-called Muret Unit is made of different tectonic slices: some of them were buried at coesite stability conditions, while oth-

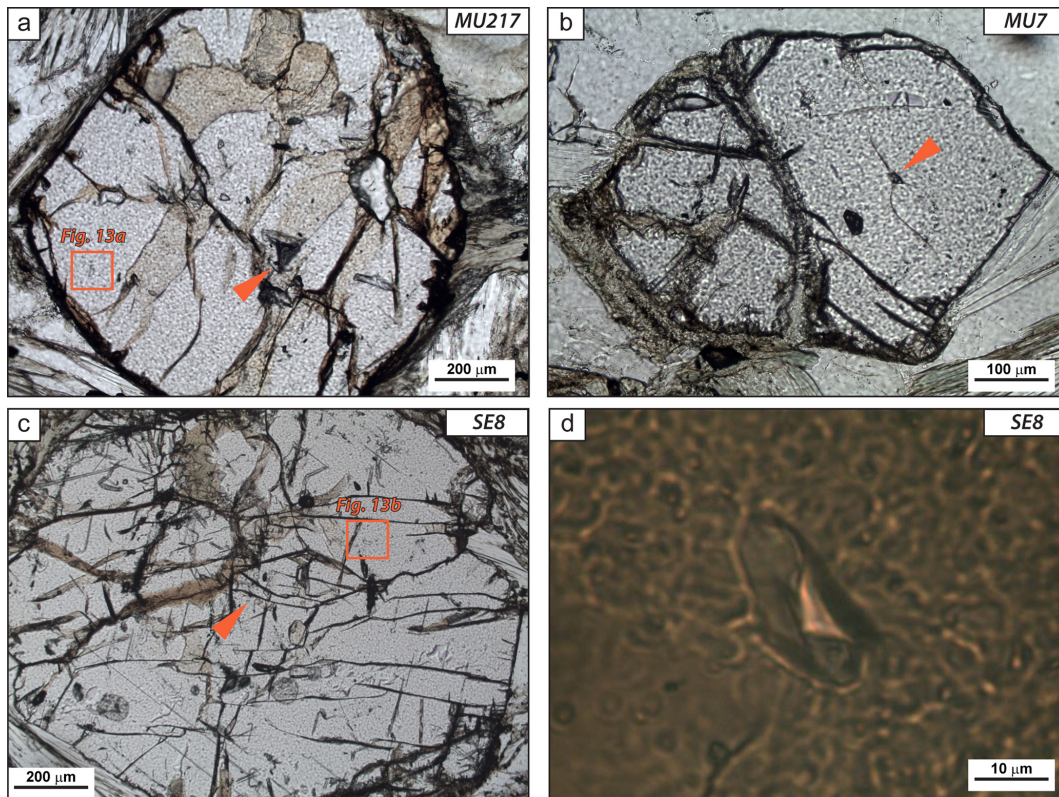


Figure 12. (a) Garnet porphyroblast from sample MU217 displaying coesite inclusions in the inner (orange arrow) and outer core (orange square). The large inclusion located in the right part of the garnet is made of a polycrystalline aggregate of quartz. (b) A tiny coesite inclusion in garnet (sample MU7) surrounded by curved cracks. (c) Large garnet porphyroblast from sample SE8 displaying several coesite inclusions in the inner and outer core (orange arrow and square). (d) A closer look at the coesite crystal included in the garnet porphyroblast shown in Fig. 8a (sample SE8).

ers were buried at lower depths (i.e. much below the quartz–coesite equilibrium). The two types of units were stacked together at a later stage during decompression. However, field observations have not been able to identify a high-strain, mylonitic, zone between those parts of the Muret Unit that contain coesite and those parts that are devoid of coesite and preserve large amounts of pre-Alpine garnet. Interestingly, we notice that high-Si muscovite is present in the coesite-absent rocks from the Muret Unit and that previous modelling failed to explain this (see Nosenzo et al., 2023). We shall come back to this point later in the discussion.

2. Differences in bulk-rock compositions may also explain why some rocks develop coesite and others not. However, all studied rocks are silica-rich metapelites of rather similar bulk-rock compositions, and thermodynamic modelling indicates that they were saturated with either quartz or coesite (see Fig. S19). Amongst these micaschists, some differences in alumina are present, but the whole-rock FeMg ratio is quite similar (Table S6). However, the storage of many elements in the pre-Alpine garnet modifies the effective bulk-rock com-

position (Fig. S19), an effect that will be explored in some detail below.

3. The calculated phase diagrams are based on equilibrium thermodynamics, an assumption that needs to be carefully evaluated. Indeed, departures from the equilibrium modelling may explain the observed inconsistencies, considering, for example, (i) that significant overstepping prevented the growth of garnet in the coesite-stability field in some rocks, explaining therefore the lack of coesite preservation in these rocks, and (ii) that the lack of a fluid phase at peak UHP conditions impeded garnet growth and hence the possibility of storing silica inclusions.

We will therefore first discuss the P – T evolution of the studied samples using the equilibrium paradigm and then explore if departures from this equilibrium model are required in order to explain the heterogeneous distribution of coesite in the studied area.

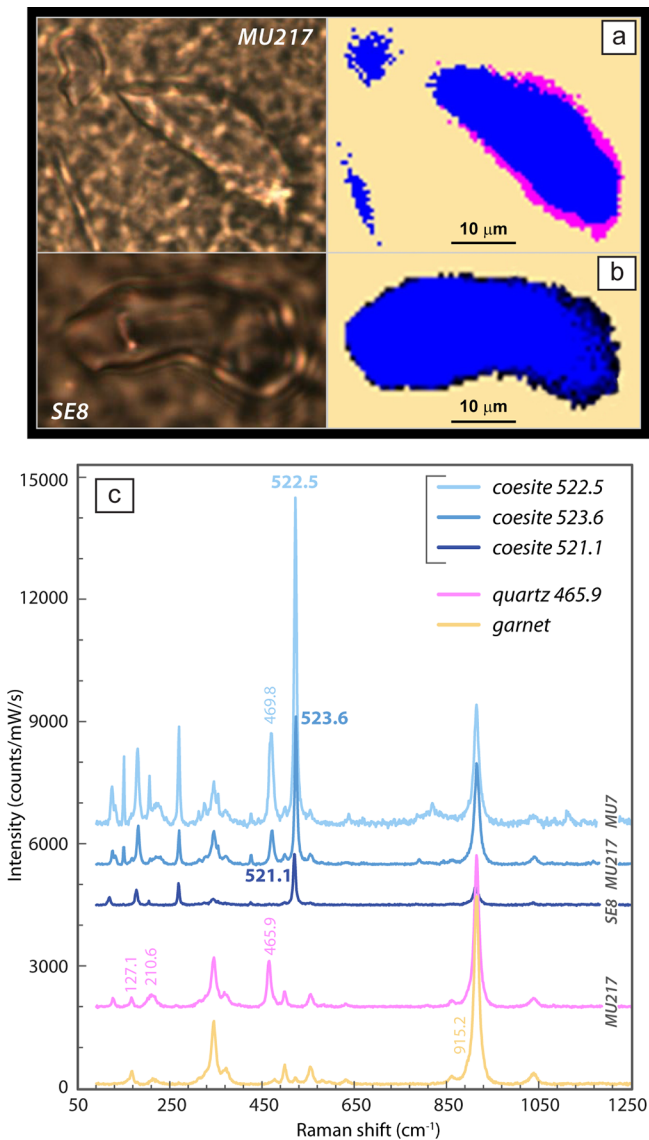


Figure 13. (a, b) Raman maps showing the distribution of coesite (in blue), quartz (in pink), and garnet (in orange). Coesite crystals are included in garnet porphyroblasts, shown in Fig. 12a and 12c. Their position within the garnet crystals is indicated by orange squares. (c) From top to bottom: Raman spectra on three coesite crystals (main peak at $\sim 521\text{ cm}^{-1}$) and quartz (main peak at $\sim 465\text{ cm}^{-1}$) hosted in garnet (main peak at $\sim 915\text{ cm}^{-1}$). Spectra are offset for clarity.

6.1 Garnet and coesite growth at equilibrium

Forward modelling based on equilibrium thermodynamics provides access, for a given bulk-rock composition, to information about (i) mineral assemblages, (ii) mineral compositions, and (iii) modal proportions, as well as their variation in a given mineral assemblage (Powell and Holland, 1990, 2010). These data may be compared with (i) the sequence of mineral assemblages observed in the rock under investi-

gation and (ii) the chemical zonation of minerals, especially garnet, where low diffusion rates allow for preservation of the growth zoning (e.g., Groppo, 2025, and references therein). Key points in constructing the phase equilibrium diagrams are (i) the choice of the effective bulk composition, including the fractionation of garnet; (ii) the assumption of a closed system, except for the fluid phase; and (iii) the assumption that the fluid phase was in excess, a reasonable inference for rocks undergoing metamorphism at increasing T . Given these premises, we have reconstructed the P – T history of the studied rocks, using first the garnet composition and then checking the predicted P – T conditions with the mineral assemblage.

6.1.1 Using predicted garnet composition

A first outcome of a phase diagram is related to garnet composition, which may be used for defining the evolution of the P – T conditions (e.g., Gaidies et al., 2006). Ideally, the isopleths for almandine, spessartine, pyrope, and grossular should intersect in a very narrow field, defining the P – T conditions at which that garnet composition was stable. Changing garnet composition gives clues to the evolution of the P – T conditions (provided garnet fractionation is taken into account). In practice, a good to excellent match of the isopleths is observed for garnet outer cores and rims (see Figs. 4, 5, 7, 9, and 10), while departures are found for spessartine and pyrope for garnet core compositions (see Figs. 4c, 7c, and 9c, discussed below). The largest discrepancy is observed between the spessartine content (spss > 40 mol %) of the garnet cores in sample SE8 and the one measured (spss = 10 mol %). This discrepancy can be attributed to (i) problems related either to the choice of the bulk-rock composition (garnet fractionation), (ii) the uncertainties affecting the modelling, (iii) thermal relaxation of the spessartine end-member (Mn being the fastest diffusing element in garnet), and (iv) overstepping in the appearance of garnet (see below).

Rather than considering individual compositions for garnet, one may rely on the relative change of end-member proportions in a garnet crystal. A notable feature in this respect is the behaviour of grossular, which remains almost constant through garnet cores, i.e. during most of the garnet growth, then slightly increases at the edge of garnet cores and strongly increases in garnet rims (Figs. 3, 6, and 8). This behaviour clearly indicates that most of the garnet cores are growing (i) in the lawsonite stability field and (ii) along a P – T path parallel to the grossular isopleths (which have moderately positive slopes) in this field. Once lawsonite is consumed, the slopes of the grossular isopleths change drastically, becoming nearly vertical, with decreasing grossular at increasing T . This peculiar behaviour results from the fact that garnet is the major Ca-bearing phase once lawsonite is consumed.

6.1.2 Using predicted mineral assemblages

A second outcome of a phase diagram is that a given garnet composition is stable in a field defined by a given mineral assemblage. Petrographic observations should be consistent with the modelled assemblage. However, it may be difficult to exactly match petrographic observations and thermodynamic predictions as some phases may be present in a very small amount in the predicted mineral assemblage (< 1 vol %–3 vol %) and may not have been detected in the thin section under petrographic investigation. Moreover, some of the predicted HP/UHP phases may have been transformed during retrogression in the matrix. A good example of this situation has been observed in sample CH11, where jadeite inclusions have been detected in rutile grains although jadeite has never been found in the matrix (Manzotti et al., 2025). In addition, coesite is predicted as a stable matrix phase at peak P – T conditions but has never been observed there, a feature common to most UHP rocks and attributed to the fast kinetics of the coesite–quartz back-reaction during decompression. Another parameter that may have a significant influence on the lack of matrix coesite is the fact that ductile deformation took place during and after garnet growth (see above). If matrix coesite has been totally lost, this is not the case for other HP/UHP phases like glaucophane. Indeed, in most of the studied samples, glaucophane pseudomorphs are still recognizable, although glaucophane itself is not present. This indicates that glaucophane was still stable at the beginning of the decompression history and has been replaced by the very fine-grained products after cessation of the ductile deformation.

6.1.3 Growth history of garnet

To sum up, in the first group of garnet-chloritoid micaschists from the Chasteiran Unit, Muret Unit, and Serre Unit, Alpine garnet crystals display similar texture, chemistry, and P – T conditions of nucleation and growth. The garnet core zonation is essentially characterized by decreasing spessartine and slightly increasing pyrope content, consistent with increasing T , and almost constant grossular content, indicating increasing P – T conditions. Thermodynamic modelling indicates that garnet cores started to grow in the quartz stability field or at the quartz–coesite transition at 2.5–2.7 GPa and 470–530 °C, along an up- P and up- T path. Its growth culminated at 2.9–3.0 GPa and 530–550 °C in the coesite–chloritoid stability field. Peak burial conditions are therefore very similar and modelled in P – T conditions of 0.1 GPa and 20 °C. These P – T values are considered within the uncertainties accepted for thermodynamic modelling. With the exception of sample MU7, all the studied samples also display a second stage of garnet growth (i.e. garnet Ca-rich rims), which developed during decompression in the quartz stability field (from 2.4–1.5 GPa) and during slight cooling (540–500 °C).

6.2 Departures from equilibrium and their potential consequences for garnet and coesite growth

6.2.1 Magnitude of potential overstepping

The P – T evaluations above have been made assuming the equilibrium paradigm. However, all metamorphic reactions require some degree of overstepping (e.g., Spear, 2017; Gaidies and George, 2021). The magnitude of this overstepping is a function of several parameters, like the Gibbs free energy difference between products and reactants, the rate of P – T change with respect to the rate of nucleation and growth of the products, and the rate-limiting processes for nucleation and growth. The question is, therefore, to evaluate how much overstepping has occurred in the studied rocks and if differences in overstepping may explain the heterogeneous distribution of coesite (the latter being found only in rocks where overstepping was negligible). Several methods for evaluating the overstepping have been proposed.

1. A first approach is to compare field observations with model predictions. This has been applied to contact metamorphic aureoles, where the observed pattern of isograds has been compared with the predictions of models of T distribution (Waters and Lovegrove, 2002; Pattison and Tinkham, 2009). This approach is not possible in the studied area, because the thermal structure during subduction has been largely modified during exhumation, and because the thermobaric structure at the time of the subduction cannot be modelled appropriately, i.e. in a reference frame that could be tied with the actual field structure.
2. A second approach is to compare the P – T conditions deduced from the location of the intersecting isopleths for the garnet core with the predicted mineral assemblage and/or the location of the garnet-in line. For example, Tamang et al. (2023) observed that the garnet core composition was in some samples stable in a field whose mineral assemblage was not the one observed when the core was growing and that the Mn content of the garnet core does not match the one calculated along the garnet-in line. Based on these observations, they suggest some degree of overstepping when garnet nucleates, but a decreasing amount of overstepping (or even no overstepping at all) when garnet reaches its final composition.

In short, in the equilibrium paradigm, nucleation of garnet should begin along the garnet-in line, and the garnet cores from the largest grains should have the same chemistry as the one predicted at the point where the P – T path is crossing this line. Departures from this point may be due to several factors, and the two groups of garnet-chloritoid micaschists will be considered successively.

6.2.2 Garnet growth in rocks devoid of pre-Alpine relicts

In the northern Dora-Maira Massif, the first group of garnet-chloritoid micaschists does not show evidence of a pre-Alpine assemblage (e.g. sample CH11 of Manzotti et al. (2022, 2025); samples MU7, MU23, and SE8 in this study). In these rocks, model predictions indicate that the garnet-in line occurs in an interval of ~ 60 °C and ~ 0.2 GPa, depending on the bulk-rock composition, in particular their Mn content. Specifically, in sample SE8 (Serre Unit), which displays the highest Mn content (spss = 0.25 mol %), garnet starts to grow at ~ 480 °C at ~ 2.5 GPa in the quartz stability field, which is 30 °C above the garnet-in line. In samples with a lower Mn content, garnet starts to grow at ~ 510 °C at ~ 2.6 GPa (sample MU23) and at ~ 500 °C at ~ 2.7 GPa (sample MU7), which is very close to the garnet-in line and just below or nearly along the quartz–coesite equilibrium.

The difference between the composition of garnet along the garnet-in line and the one observed in garnet cores may be due to the fact that the garnet grains investigated in a specific thin section were not cut through their true centre; therefore, their chemistry does not reflect the one that was stable when the first garnet was formed. Another classic explanation for this discrepancy is our imperfect knowledge of the solid solution models for garnet. Other explanations may involve consideration of the possibility that garnet nucleation took place over a range of T (George and Gaidies, 2017) or problems with the definition of the effective equilibration composition (Lanari and Engi, 2017). Overall, we consider that the observed discrepancies, not always present, are within the uncertainties of the equilibrium thermodynamic models and do not provide a clear-cut argument in favour of overstepping.

6.2.3 Garnet growth in polycyclic rocks

In polycyclic rocks, large garnet grains from a previous orogenic cycle can store a significant amount of material, especially Mn (e.g., Ganne et al., 2003; Le Bayon et al., 2006; Feenstra et al., 2007; Gaidies et al., 2008; Giuntoli et al., 2018; Nosenzo et al., 2022, 2023). Therefore, fractionation of the pre-Alpine garnet drastically changes the effective bulk-rock composition (Fig. S19). In addition, in such samples, Alpine garnet may not nucleate as new crystals in the matrix but grow as inclusion-free thin rims around pre-Alpine garnet or sealed fractures that dissected pre-Alpine garnet.

In the Muret Unit, thermodynamic modelling of the polycyclic rocks constrains the growth of Alpine garnet at 2.1–2.2 GPa and 530–560 °C in the quartz stability field (Nosenzo et al., 2023). These P – T estimates are comparable, within uncertainties, with the P – T conditions of the second stage of garnet growth described in our study and in Manzotti et al. (2022, 2025). Up to now, coesite has not been found in these samples. It is, however, conceivable that the polycyclic rocks share the same P – T evolution as the other rocks and

that garnet may not have been stable at peak (UHP) conditions because of the large effect induced by the storage in the pre-Alpine garnet of key elements (Mn, Ca) stabilizing garnet at UHP. In this situation, Alpine garnet cannot store coesite.

To evaluate this hypothesis, we performed new calculations in the P – T range 1.5–3.0 GPa and 450–600 °C on the same three samples (i.e. GM1, GM2, and GM13) studied by Nosenzo et al. (2023), adopting the approach used in this study (see Sect. 3.3). This will allow for comparing the P – T conditions inferred for the growth of garnet in polycyclic rocks in the Muret Unit, with the ones estimated in this study for samples displaying only the Alpine garnet generation. The main outcomes of these new calculations are briefly summarized below. We refer to Nosenzo et al. (2023) for a detailed description of the chemistry and texture of garnet present in the modelled rocks.

- In sample GM1, Alpine garnet (alm₇₅prp₁₄grs₆) seals fractures that cut across centimetre-sized pre-Alpine garnet porphyroblasts (Fig. 4 in Nosenzo et al., 2023). The intersection of chemical isopleths constrains the P – T conditions of garnet growth in a narrow field at ~ 1.9 GPa and 540–550 °C in a lawsonite-absent field. These P – T estimates are consistent with the ones (orange rectangle in Fig. 14a) obtained by Nosenzo et al. (2023), although P values are slightly lower.

The P – T path (blue arrows in Fig. 14) inferred from the garnet growth at the quartz–coesite transition in the Muret Unit (samples MU23 and MU7, this study) falls in a garnet-free P – T space and crosses the garnet-in line only during decompression at ~ 2.5 GPa and ~ 540 –550 °C. The absence of the garnet growth at the quartz–coesite transition in sample GM1 can therefore be explained by its effective bulk-rock composition, allowing for the growth of garnet only at ~ 540 –550 °C. It is worth noting that sample GM1 contains muscovite with high Si content (GM1 Si up to 3.58 a.p.f.u.), which is predicted to be stable at much higher P conditions than those of the Alpine garnet, in the coesite stability field.

- In sample GM2, Alpine garnet overgrows clasts of pre-Alpine garnet, mainly in the outer portion of large pre-Alpine garnet porphyroblasts (Figs. 5 and 6 in Nosenzo et al., 2023). Alpine garnet forms a very thin and irregular corona (i.e. Alpine garnet core, alm: ~ 68 mol %, prp: ~ 10 mol %, grs: ~ 20 mol %) around the pre-Alpine clasts surrounded by a thicker and idioblastic rim (alm: ~ 79 mol %, prp: ~ 18 mol %, grs: ~ 3). Garnet chemical isopleths (grossular and almandine) constrain the growth of the garnet core and rim, at ~ 1.6 GPa and ~ 510 °C and at ~ 2.1 GPa and ~ 550 °C, respectively. As already noted by Nosenzo et al. (2023), the pyrope

isopleth (prp: 8 mol %) for the garnet core does not fit the measured pyrope composition (11 mol %).

Our modelling is compatible with the growth of the garnet core along a prograde P – T in the quartz stability field. The garnet-in line is located at $\sim 490^\circ\text{C}$ at ~ 1.5 GPa and at $\sim 530^\circ\text{C}$ at ~ 2.8 GPa, crossing the lawsonite-out line at $\sim 520^\circ\text{C}$ and ~ 2.1 GPa. The P – T path (blue arrows in Fig. 14b) inferred from the garnet growth at the quartz–coesite transition in the Muret Unit (samples MU23 and MU7, this study) falls in a garnet-free P – T space and crosses the garnet-in line only at ~ 2.8 GPa and ~ 530 – 540°C . Therefore, assuming equilibrium thermodynamics and that sample GM2 followed a P/T gradient similar to the rocks containing coesite, a relative low modal amount of garnet (~ 1 mol %) should have formed at the quartz–coesite transition. However, sample GM2 does not contain garnet with a composition compatible with its growth at UHP conditions. Its absence can be explained by T overstepping of garnet growth or by the attainment of the 0.5 vol % threshold of garnet modal amount, below which garnet is undetectable in thin section (Nagurney et al., 2021). As already noted for sample GM1, sample GM2 displays muscovite with high Si content (GM2 Si up to 3.59 a.p.f.u.), which is predicted to be stable at much higher P conditions than the ones of the Alpine garnet in the coesite stability field.

Finally, our modelling suggests that garnet rims grew at P – T conditions similar to the ones estimated by Nosenzo et al. (2023) as well as to the ones estimated for garnet rims in rocks devoid of pre-Alpine relicts. Its growth may have, therefore, occurred during decompression.

- In sample GM13, Alpine garnet forms thin and discontinuous overgrowths around pre-Alpine garnet porphyroblasts (Fig. 8 in Nosenzo et al., 2023). Garnet displays a core-to-rim decrease in grossular (19 mol %–9 mol %) and pyrope (11 mol %–9 mol %) compensated by an increase in almandine (69 mol %–80 mol %). Garnet chemical isopleths (grossular and almandine) constrain the growth of the garnet core and rim in lawsonite-present fields, at ~ 1.9 GPa and $\sim 470^\circ\text{C}$ and at ~ 2.5 GPa and $\sim 530^\circ\text{C}$, respectively.

Our modelling is compatible with the growth of the garnet core along a prograde P – T in the quartz stability field (Fig. 14c–d). The garnet-in line is located at $\sim 460^\circ\text{C}$ at ~ 1.5 GPa and at $\sim 480^\circ\text{C}$ at ~ 3.0 GPa. Therefore, assuming equilibrium and that sample GM13 followed a P – T gradient similar to the rocks containing coesite, a relative low modal amount of garnet (~ 1 mol %) should have formed at the quartz–coesite transition. However, sample GM13 does not contain gar-

net with a composition compatible with growth at UHP conditions.

6.2.4 Availability of H_2O at peak UHP conditions

Many previous studies have emphasized the role of the fluid phase in the effective production of mineral assemblages (Heinrich, 1982; Guiraud et al., 2001; Proyer, 2003; Tenczer et al., 2006; Schorn, 2018, 2022; Luisier et al., 2023). These studies have shown that new mineral assemblages develop at increasing P – T conditions if dehydration is taking place (e.g., in a mudstone saturated in H_2O). Given that most H_2O produced will escape the rock, the preservation of the peak assemblage depends on the amount of fluid that is introduced into the rock during exhumation. On the contrary, new mineral assemblages do not grow if a large amount of hydration is required during the prograde P – T path (e.g., in an unaltered gabbro or granite). Along this line of reasoning, the studied monocyclic metapelites were probably saturated in water during their prograde path, leading to garnet growth across the quartz–coesite transition. The polycyclic metapelites have been largely dehydrated before the Alpine orogeny, as shown in a previous detailed study (Nosenzo et al., 2023). According to these authors, a fluid phase will be present in the polycyclic metapelites only if some water is added to the system either during the retrograde pre-Alpine history or during the prograde Alpine history. The same result is obtained whether the peak P – T conditions are estimated at 2.1–2.2 GPa and 530–560 $^\circ\text{C}$ (Nosenzo et al., 2023) or at 3.0 GPa and 530–560 $^\circ\text{C}$, as recalculated in this study (Fig. S20). We note that the Alpine overgrowths in the polycyclic metapelites record similar P – T conditions than garnet rims in the rocks devoid of pre-Alpine relicts. In this hypothesis, the garnet overgrowths may record a transient episode of fluid infiltration during exhumation (Manzotti et al., 2025).

Overall, the thermodynamic modelling for the micaschists displaying pre-Alpine garnet is much less satisfactory than for the first group of garnet-chloritoid micaschist. Difficulties in modelling polycyclic rocks have also been encountered by other workers, and we concur with George et al. (2024) that “a potential combination of the paucity of the fluid, limited strain accumulation, and coarse refractive assemblages stabilized a kinetically sluggish and metastable composition”. In our case, most of the polycyclic Muret rocks display limited Alpine strain, and pre-Alpine garnet is a coarse refractive mineral. For kinetic reasons, garnet may not have grown whilst the rocks were in the coesite stability field, and only limited Alpine garnet mainly grew during decompression, possibly due to an episode of fluid flux (see also Nosenzo et al., 2023).

Muret Unit – Rocks with polycyclic garnet

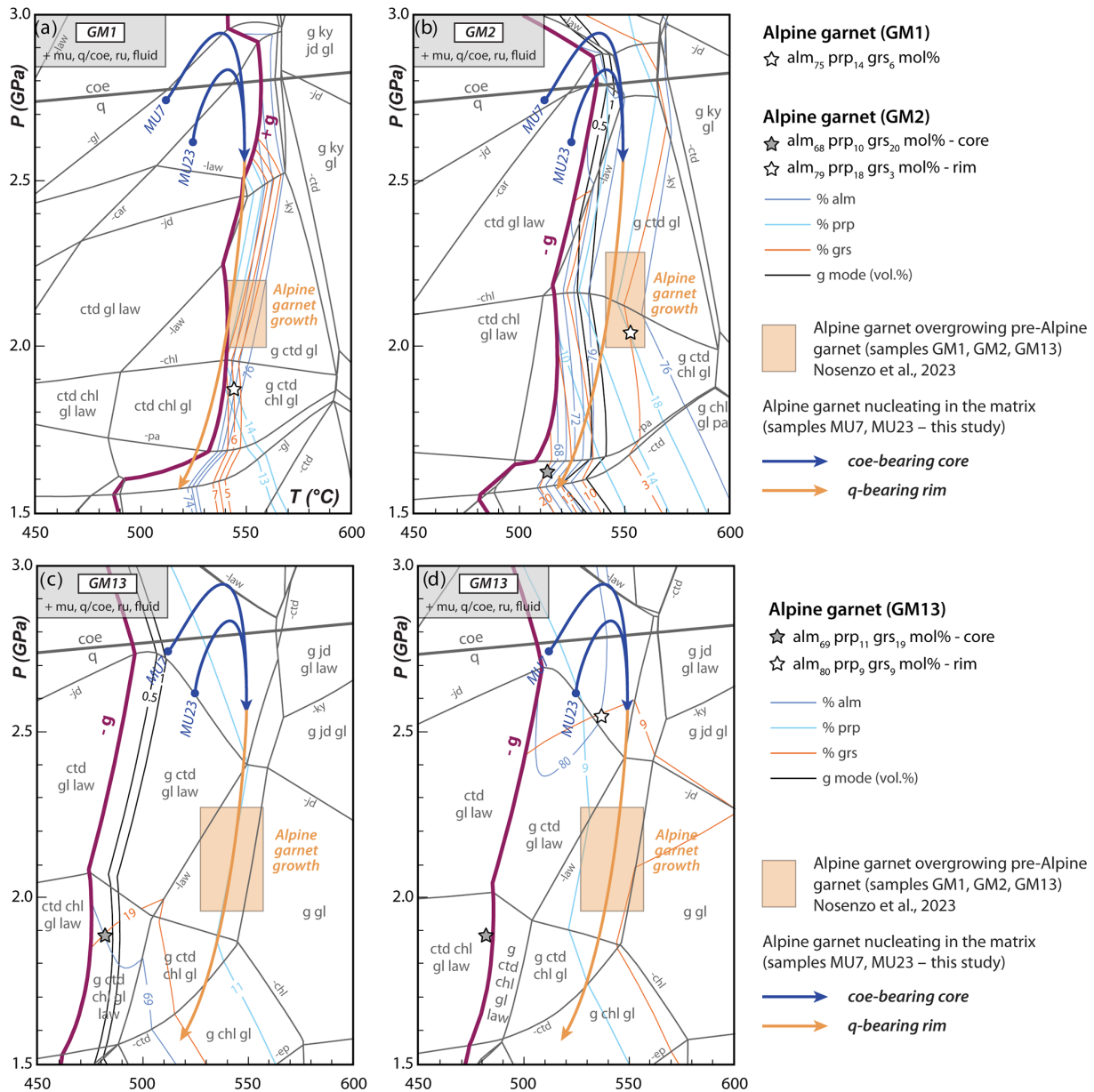


Figure 14. (a, b, c, d) P – T phase diagrams for the growth of Alpine garnet (grey and white stars) in the polycyclic rocks from the Muret Unit: sample GM1 (a), GM2 (b), and GM13 (c, d), calculated using H_2O in excess. Alpine garnet core fractionation has been considered only for sample GM13 (Fig. 14d), due to the very small amount of Alpine garnet in the other samples. Some fields are not labelled for the sake of clarity; their assemblages can be deduced from the assemblages in adjacent fields. The blue and orange arrows indicate the P – T conditions for the growth of the core and rim of Alpine garnet in monocyclic Muret samples, respectively, as inferred from this study. The orange rectangles indicate the P – T conditions of garnet growth estimated by Nosenzo et al. (2023).

6.3 Garnet growth in low-temperature HP/UHP metapelites: an overall assessment

Numerous examples of garnet-bearing metapelites have been reported worldwide in HP/UHP terrains, and a large number of them have been analysed through equilibrium thermodynamic modelling. Based on our experience and a literature

survey, we stress below some of the major conclusions of these studies (Fig. 15a). To offer a basis for comparison, a phase diagram for an average pelite (Forshaw and Pattison, 2023; Table S10) was calculated in the P – T range of 1.5–3.5 GPa and 400–700 °C (Fig. 15c). Obviously, this model phase diagram is constructed assuming excess H_2O , and – by

definition – it is only valid for that specific bulk-rock chemistry. However, our purpose here is to summarize the main behaviour common to most metapelites displayed on this diagram. Finally, we keep in mind that part of the diagram (out of scope of this study) will be metastable with respect to melting reactions.

For the sake of clarity, it is convenient to divide the phase diagram in four main domains: garnet-absent assemblages at low T (domain I), garnet–chloritoid–lawsonite assemblages (domain II), garnet–chloritoid without lawsonite assemblages (domain III), and garnet–kyanite assemblages (in most cases without lawsonite) (domain IV). In this model system, garnet appears at about 460 °C, in the lawsonite stability field. This value is dependent on the amount of MnO in the bulk-rock composition; the lower the amount of MnO, the higher the T of garnet nucleation. In addition, the effect of Mn fractionation in garnet cores, observed in all investigated rocks, is to displace this garnet-in line towards slightly higher T , an effect that is well described not only in HP rocks but also at medium-to-low P (Tinkham et al., 2001; Tinkham and Ghent, 2005; Zuluaga et al., 2005). Garnet zoning in most HP metapelites is characterized by a bell-shaped Mn curve and a nearly constant Ca content. This indicates that garnet nucleation and subsequent growth has taken place in domain II. This has major implications in terms of P – T evolution, because in domain II, spessartine isopleths are nearly parallel to the garnet-in line, whereas the grossular isopleths display moderate positive slopes. The amount of grossular is a first indication of the P at which garnet nucleates in domain II. This behaviour is observed in all calculated phase diagrams in this study (Figs. 4, 5, 7, 9, and 10) and has also been observed in other garnet–chloritoid metapelites from the northern Dora-Maira Massif (Gasco et al., 2011; Manzotti et al., 2022; Nosenzo et al., 2023), from the Gran Paradiso Massif (Le Bayon et al., 2006; Manzotti et al., 2015, 2024), from the Sesia Zone (Regis et al., 2014), and from the Variscan belt (López-Carmona et al., 2010; Cruciani et al., 2013).

Once lawsonite is consumed (domains III and IV), garnet growth continues given an appropriate P – T path. However, the shape of the grossular isopleths has drastically changed, becoming steeply negative. This means that along a prograde (i.e. increasing both in T and P) path, the zoning of garnet is characterized by a decrease in grossular. In these domains, III and IV, the grossular content of garnet cannot be used for P estimations but decreases with increasing T . Note that the pyrope content in domains II, III, and IV is increasing with increasing T , consistent with the fact that most garnet crystals in HP/UHP metapelites display a regular increase in pyrope content. In particular, this smooth increase does not show any discontinuity when crossing the region where grossular begins to decrease (i.e. the lawsonite-out line).

The quartz–coesite transition has a slight positive slope (e.g. Bose and Ganguly, 1995), and it may be crossed by the P – T path either in domain II or domain IV. A small, but significant, number of studies have reported this transition “fos-

silized” in garnet, in which case garnet cores display quartz inclusions, whereas garnet rims display coesite inclusions (or its breakdown product, namely quartz). Reports of this texture can be found in Reinecke (1998), Parkinson (2000), Manzotti et al. (2022), and Ghignone et al. (2023). The preservation of quartz inclusions in garnet cores is generally ascribed to the armouring (in a mechanical sense) effect of garnet, a much stiffer mineral than the surrounding matrix. If at equilibrium, all silica in the matrix should be coesite, which means that 20 to 30 vol % of garnet–chloritoid micaschist was made of coesite (see Figs. 4, 7, and 9). In a few cases, the silica polymorph in the garnet core is coesite (Ghignone et al., 2024; Groppo et al., 2025), suggesting that the garnet-forming reaction took place in the coesite stability field or that some overstepping took place. This means that some rocks may have crossed the quartz–coesite transition at a rather low T , below the garnet-in line. Provided this is not due to a particularly low amount of Mn in the bulk composition, it also opens a window for future studies, aiming at providing evidence for coesite-bearing carpholite and/or chloritoid assemblages at very low T (400–450 °C).

Strictly speaking, an isochemical phase diagram is only valid for one bulk composition. In the case of Fig. 15, we used the average pelite of Forshaw and Pattison (2023), which is a low Ca pelite (CaO = 0.65 wt %, Fig. 16a and Table S10) with an Mg# of 0.38 (Fig. S21a). In order to explore the potential effect of departures from this average pelite, we have calculated other phase diagrams, changing either the Ca content (Fig. 16b–c) or the Mg# (Fig. S21). In particular, increasing the CaO content (from 0.65 wt %–2.50 wt %) will displace the garnet-in line towards lower T (up to 50 °C) and the lawsonite-out line towards slightly higher T . The grossular isopleths are not significantly changed, both with respect to their slopes and values (Fig. 16b). The same behaviour is observed for the pyrope isopleths (Fig. 16c). It follows that minor changes in CaO with respect to the average pelite does not change the main conclusions, i.e. that the grossular content within garnet cores is a first-order indication of the P at which this phase has nucleated. By contrast, increasing the Mg# has the opposite effect than increasing the CaO content of the bulk composition: the garnet-in line is moved towards higher T with increasing Mg# (Fig. S21). In addition, the location of the pyrope isopleths is modified, and the garnet composition for a given P – T point changes (i.e. its pyrope content increases at increasing Mg#). Overall, the effect of the Mg ratio is larger than the one for CaO.

6.4 Some tectonic implications for the Dora-Maira Massif

A few years ago, UHP metamorphism in the Dora-Maira Massif was restricted to the Brossasco-Isasca Unit, in its southern part (from Chopin, 1984 to Groppo et al., 2019). In the northern Dora-Maira Massif, the discovery of a thin layer of garnet–chloritoid micaschist (the Chasteiran Unit) contain-

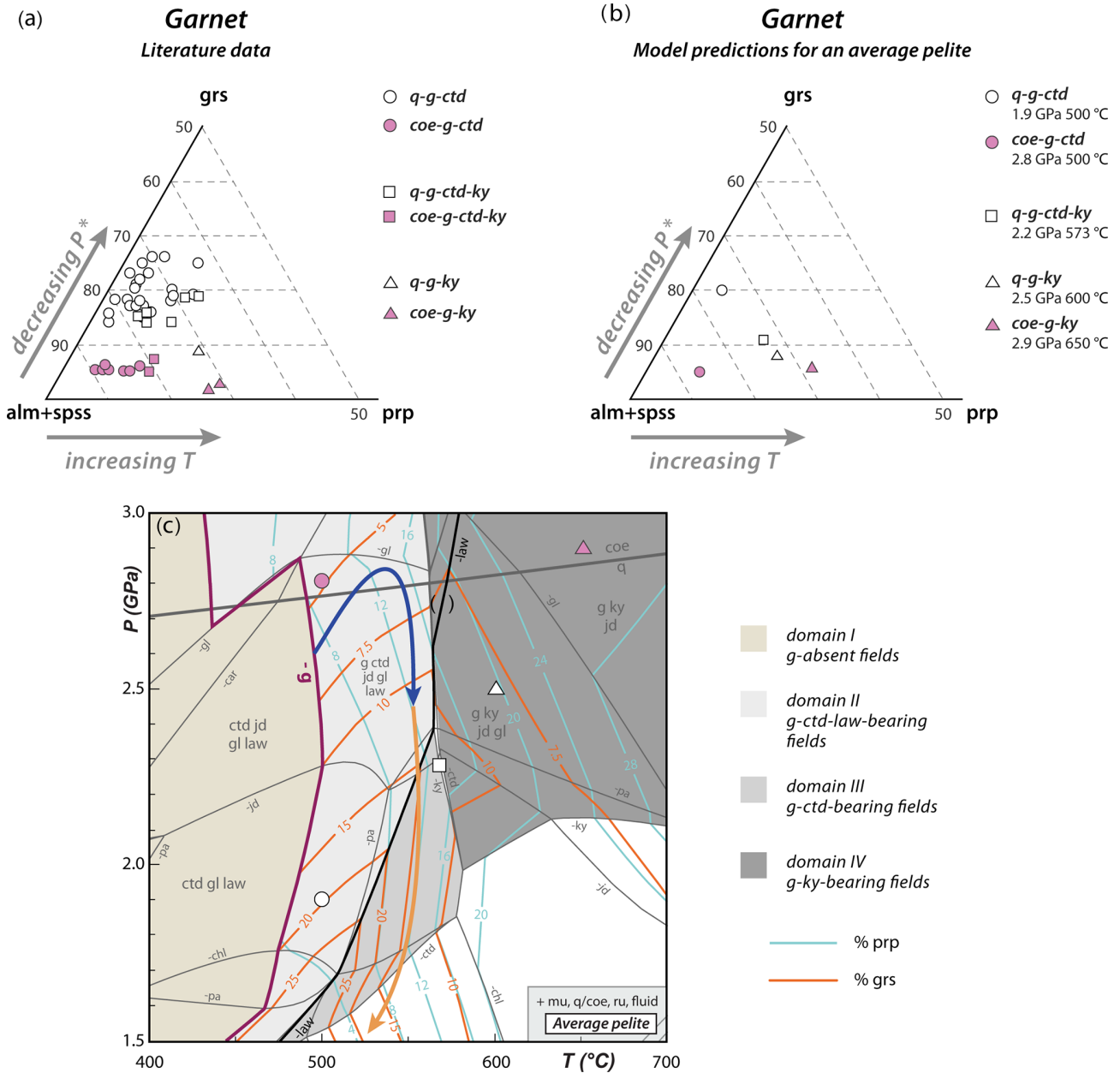


Figure 15. (a, b) Range of chemical composition of garnet from metapelites, plotted in the (alm + spss)–grs–prp diagram. (a) Data are from this study and a literature compilation. Alpine belt (Vuichard and Ballèvre, 1989; Meyre et al., 1999; Ganne et al., 2003; Le Bayon et al., 2006; Hoschek et al., 2010; Smye et al., 2010; Gasco et al., 2011; Regis et al., 2014; Manzotti et al., 2015; Groppo et al., 2016, 2019; Manzotti et al., 2022; Nosenzo et al., 2023; Groppo et al., 2025), Variscan belt (Guiraud et al., 1987; Ballèvre et al., 1989; Bosse et al., 2002; Jouvent et al., 2022; López-Carmona et al., 2013; Žáčková et al., 2010; Szczepański et al., 2022), Carpathians (Negulescu et al., 2018), Uralian belt (Schulte and Blümel 1999), Aegean belt (Katagas, 1980), Qilian orogen (Wei and Song, 2008), Guatemala Suture Zone (Maldonado et al., 2016), Rhodope Zone (Mposkos and Liati, 1993), Himalayan belt (Guillot et al., 1997), Raspas Complex (Gabriele et al., 2003), Kokchetav Massif (Parkinson, 2000), and Kyrgyz Tian Shan (Orozbaev et al., 2015). (b) Data were calculated by thermodynamic modelling using the bulk composition of the average pelite from Forshaw and Pattison (2023). * Please note that “decreasing in *P*” in both diagrams refers only to lawsonite-present fields (i.e. domain II). (c) H₂O-saturated *P*–*T* phase diagrams were calculated using the bulk composition of an average pelite (Forshaw and Pattison, 2023). Some fields are not labelled for the sake of clarity; their assemblages can be deduced from the assemblages in the adjacent fields. The blue and orange arrows indicate the *P*–*T* conditions for the growth of the garnet cores and rims, respectively, as inferred from the samples investigated in this study. Chemical isopleths for garnet (grossular and pyrope) are also shown. Circle, square, and triangle symbols indicate the *P*–*T* conditions to which the garnet compositions have been plotted in Fig. 15b.

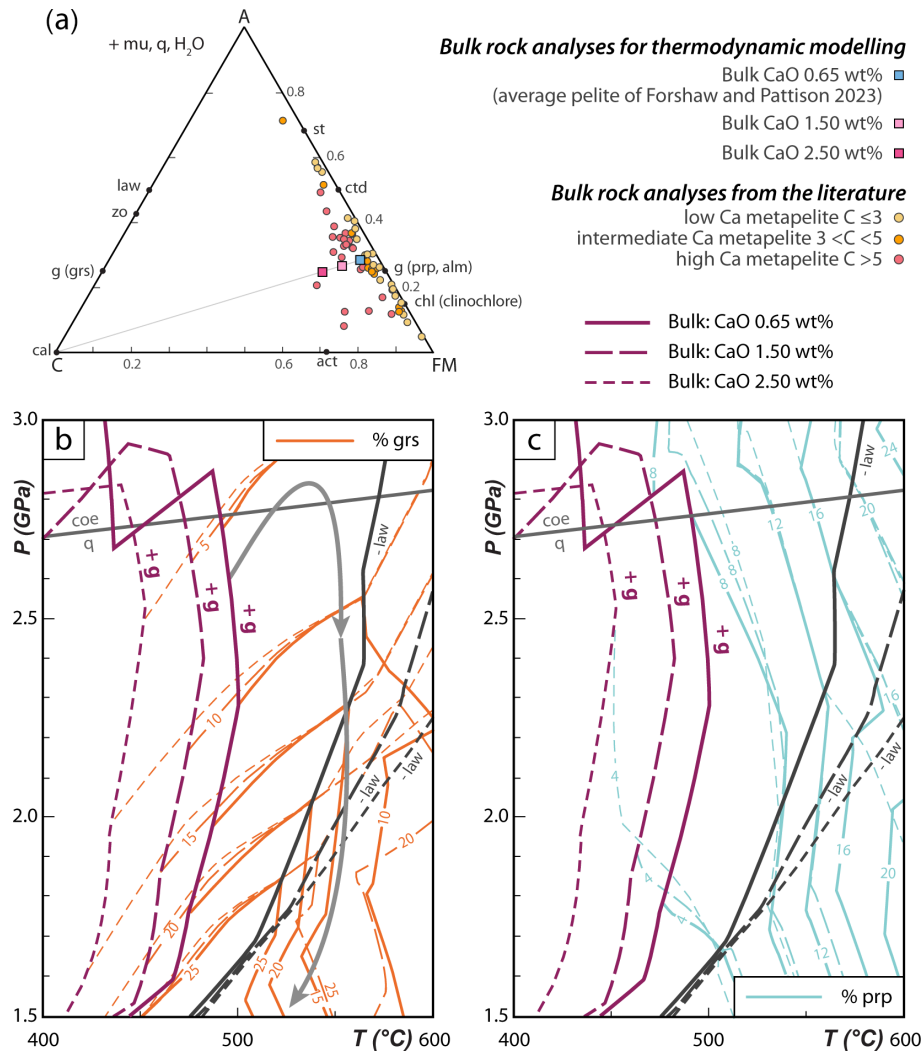


Figure 16. (a) AC(FM) projection of bulk-rock chemical analyses (in mol %) of metapelites. Colours refer to the amount of CaO in the bulk, arbitrarily divided into three groups (see Groppo et al., 2025). Data are from a literature compilation (see caption of Fig. 15 for details). (b, c) P–T diagrams displaying (for three different bulk-rock compositions, plotted (squares) in the AC(FM) diagram above) the garnet-in and lawsonite-out lines, and the isopleths for grossular content (b) and pyrope content (c) in garnet. Note that the change of bulk-rock chemistry has a significant effect on the location of the garnet-in and lawsonite-out lines and much less effect on the location of the grossular and pyrope isopleths.

ing coesite was unexpected (Manzotti et al., 2022, 2025). Re-examination of samples in the southern Dora-Maira Massif has allowed Groppo et al. (2025) to distinguish a new tectonic unit, the Rocca Solei Unit. In this study, we proceed further on the analysis of the extent of the UHP metamorphism by describing other occurrences of coesite in the garnet-chloritoid micaschists from the Muret Unit, a slice of Palaeozoic basement, but also in those from the Serre Unit, considered the cover of the Palaeozoic basement. This study therefore enlarges considerably the volume of the rocks affected by the UHP metamorphism in the Dora-Maira Massif, albeit at different metamorphic grades. The Brossasco-Isasca remains a distinctive unit, because its metamorphism

took place at very high P and T (4.0–4.3 GPa, 700–730 °C), epitomized by the *coesite–kyanite eclogite facies*. The other units (Chasteiran, Rocca Solei, and now Muret and Serre) are characterized by the stability of Fe-rich chloritoid and grossular-poor garnet in the coesite stability field and are, therefore, associated under the heading of *coesite–chloritoid eclogite facies*. Lower P–T conditions are recorded by these rocks, which equilibrated at the transition from quartz to coesite (i.e. ~2.9 GPa, 530–550 °C).

Mapping the areal extent of these two eclogite facies at the scale of the Dora-Maira Massif will require time-consuming field studies. Our present knowledge is quite good in the southern Dora-Maira Massif (i.e. in the Varaita and Po val-

leys), as well as in the northern part of the massif (i.e. in the Chisone and Germanasca valleys). A large gap in our knowledge is present in the central part of the massif, i.e. between the Po and the Pellice valleys. Figure 1 summarizes the present state of knowledge. The lowest unit is the Sanfront-Pinerolo Unit, well identified in the Po, Germanasca, and Chisone valleys, metamorphosed at ~ 2.0 GPa (Grosso et al., 2019). Most slices thrust on top of the Sanfront-Pinerolo Unit record UHP conditions (Brossasco-Isasca and Rocca Solei to the south; Chasteiran, Muret, and Serre to the north). For the sake of clarity, the smaller units, namely the San Chiaffredo, Grimbassa, and Serre, have not been shown in Fig. 1. A more serious problem results from our poor state of knowledge in the central part of the Dora-Maira Massif. We have chosen to make one single UHP unit from the north (Muret) to the south (Ricordone), awaiting future studies. One can be, however, confident that an adequate representation of the extent of the UHP metamorphism will be found in the near future, because low-Ca metapelites displaying garnet–chloritoid–(lawsonite) assemblages are widespread in both the central (Pellice Valley: Scaillet et al., 1992) and southern part (Po Valley: Caso et al., 2024). One may also emphasize that the tectonic boundary between the lower Sanfront-Pinerolo and higher UHP units, a top-to-West ductile shear zone (Avigad et al., 2003; Nerone et al., 2024), represents the major gap in the metamorphic structure of the Western Alps, because the section missing along this contact represents a difference in depth along the subduction zone of the order of 30 to 60 km.

7 Conclusions

This study leads to the following main conclusions.

In the garnet–chloritoid micaschist from the northern Dora-Maira Massif, evidence for UHP conditions is more widespread than previously thought, based on thermodynamic modelling of garnet composition and Raman characterization of coesite.

According to thermodynamic modelling, garnet begins to grow at slightly lower P than the quartz–coesite equilibrium, continues into the coesite stability field, and achieves its growth during slight decompression that ends in the quartz–stability field. The distribution of the quartz and coesite inclusions in garnet is consistent with thermodynamic modelling.

Although some overstepping is a necessary requirement in all metamorphic reactions, it was not a major parameter in the three new samples investigated in this contribution or our previous study (Manzotti et al., 2022). Slight differences in P – T paths between samples are within the uncertainties of the thermodynamic calculation.

The only exception to this rule has been observed in the garnet–chloritoid micaschist preserving evidence of polycyclism (large pre-Alpine garnet grains and staurolite pseudo-

morphs). This may be related to the details of the reaction mechanisms, especially the timing and amount of fluid access inside the system, and the consequent changing scale of the effective bulk compositions during garnet growth.

Preserved growth zoning in garnet is a powerful tool to understand the P – T path, especially when the quartz–coesite boundary is crossed along this P – T path. The consistency between (i) the measured chemical composition and the observed distribution of quartz/coesite inclusions, on the one hand, and (ii) equilibrium thermodynamic predictions, on the other hand, suggests, once again, minimal departures due to overstepping.

Data availability. All data related to this article can be found in the Supplement.

Supplement. The supplement related to this article is available online at <https://doi.org/10.5194/ejm-37-455-2025-supplement>.

Author contributions. PM: conceptualization, funding acquisition, investigation (fieldwork, mineralogical and petrological data acquisition, thermodynamic modelling), figures preparation, writing (original draft). FS: investigation (mineralogical acquisition), writing (review and editing). MB: investigation (fieldwork), writing (original draft). FN: investigation (fieldwork). All authors contributed to the discussion and read and approved the final version of the manuscript.

Competing interests. The contact author has declared that none of the authors has any competing interests.

Disclaimer. Publisher's note: Copernicus Publications remains neutral with regard to jurisdictional claims made in the text, published maps, institutional affiliations, or any other geographical representation in this paper. While Copernicus Publications makes every effort to include appropriate place names, the final responsibility lies with the authors.

Acknowledgements. Victoria Pease is thanked for providing us the XRF bulk analyses. We thank Christian Chopin and Simon Schorn for their constructive and inspiring reviews as well as Chiara Grosso and Elisabetta Rampone for editorial handling and comments. The first author warmly thanks the European Institute of Oncology (Milano) for great professional and human support. She dedicates this work to her family, the safe harbour to return to in the midst of the biggest storm of her life.

Financial support. This research was supported by the UCA (Clermont Auvergne University) “Accueil de conférenciers invités internationaux” funding programme and by Stockholm University.

The publication of this article was funded by the Swedish Research Council, Forte, Formas, and Vinnova.

Review statement. This paper was edited by Chiara Groppo and reviewed by Christian Chopin and Simon Schorn.

References

- Anderson, G.: Thermodynamics of natural systems. Theory and applications in geochemistry and environmental science, 3rd Edn., Cambridge University Press, 413 pp., <https://doi.org/10.1017/9781316796856>, 2017.
- Avigad, D., Chopin, C., and Le Bayon, R.: Thrusting and extension in the southern Dora-Maira ultra-high-pressure massif (Western Alps): view from below the coesite-bearing unit, *J. Geol.*, 111, 57–70, 2003.
- Ballèvre, M., Pinardon, J.-L., Kienast, J.-R., and Vuichard, J.-P.: Reversal of Fe-Mg partitioning between garnet and staurolite in eclogite-facies metapelites from the Champtocéaux Nappe (Brittany, France), *J. Petrol.*, 30, 1321–1349, 1989.
- Ballèvre, M., Camonin, A., Manzotti, P., and Poujol, M.: A step towards unraveling the paleogeographic attribution of pre-Mesozoic basement complexes in the Western Alps based on U-Pb geochronology of Permian magmatism, *Swiss J. Geosci.*, 113, 12, <https://doi.org/10.1186/s00015-020-00367-1>, 2020.
- Beyssac, O., Goffé, B., Chopin, C., and Rouzaud, J. N.: Raman spectra of carbonaceous material in metasediments: a new geothermometer, *J. Metamorph. Geol.*, 20, 59–871, 2002.
- Bose, K. and Ganguly, J.: Quartz-coesite transition revisited: Reversed experimental determination at 500–1200 °C and retrieved thermochemical properties, *Am. Min.*, 80, 231–238, 1995.
- Bosse, V., Ballèvre, M., and Vidal, O.: Ductile thrusting recorded by the garnet isograd from blueschist-facies metapelites of the Ile de Groix, Armorican Massif, France, *J. Pet.*, 43, 485–510, 2002.
- Bousquet, R., Oberhänsli, R., Schmid, S. M., Berger, A., Wiederkehr, M., Robert, C., Möller, A., Rosenberg, C. L., Zeilinger, G., and Molli, G., Robert, C., Wiederkehr, M., Koller, F., and Möller, A.: Metamorphic framework of the Alps. Commission for the Geological Map of the World, Subcommission for Magmatic and Metamorphic Maps, CCGM/CGMW, Paris, ISBN: 978-2-917310-17-5, 2012.
- Boyer, H., Smith, D. C., Chopin, C., and Lasnier, B.: Raman microprobe (RMP) determination of natural and synthetic coesite, *Phys. Chem. Minerals*, 12, 45–48, 1985.
- Bussy, F. and Cadoppi, P.: U-Pb dating of granitoids from the Dora-Maira massif (Western Italian Alps), *Schweiz. Mineral. Petrogr. Mitt.*, 76, 217–233, 1996.
- Carlson, W. D., Pattison, D. R. M., and Caddick, M. J.: Beyond the equilibrium paradigm: How consideration of kinetics enhances metamorphic interpretation, *Am. Mineral.*, 100, 1659–1667, 2015.
- Caso, F., Petroccia, A., Nerone, S., Maffei, A., Corno, A., and Zucali, M.: Comparison between 2D and 3D microstructures and implications for metamorphic constraints using a chloritoid-garnet mica schist, *Eur. J. Mineral.*, 36, 381–395, 2024.
- Černok, A., Boffa Ballaran, T., Caracas, R., Miyajima, N., Bykova, E., Prakapenka, V., Liermann, H.-P., and Dubrovinsky, L.: Pressure-induced phase transitions in coesite, *Am. Mineral.*, 99, 755–763, 2014.
- Chopin, C.: Coesite and pure pyrope in high-grade blueschists of the Western Alps: a first record and some consequences, *Contrib. Mineral. Petrol.*, 86, 107–118, 1984.
- Chopin, C., Henry, C., and Michard, A.: Geology and petrology of the coesite-bearing terrain, Dora-Maira massif, Western Alps, *Eur. J. Mineral.*, 3, 263–291, 1991.
- Coleman, R. G. and Wang, X.: Ultrahigh Pressure Metamorphism. Cambridge: Cambridge University Press, 528 pp., <https://doi.org/10.1017/CBO9780511573088>, 1995.
- Compagnoni, R. and Rolfo, F.: UHPM Units in the Western Alps, *EMU Notes Mineral.*, 5, 13–49, 2003.
- Connolly, J. A. D. and Cesare, B.: C-O-H-S fluid composition and oxygen fugacity in graphitic metapelites, *J. Metamorph. Geol.*, 11, 379–388, 1993.
- Cruciani, G., Franceschelli, M., Massonne, H.-J., Carosi, R., and Montomoli, C.: Pressure-temperature and deformational evolution of high-pressure metapelites from Variscan NE Sardinia, Italy, *Lithos*, 175/176, 272–284, 2013.
- de Capitani, C. and Brown, T. H.: The computation of chemical equilibrium in complex systems containing non-ideal solutions, *Geochim. Cosmochim. Ac.*, 51, 2639–2652, 1987.
- de Capitani, C. and Petrakakis, K.: The computation of equilibrium assemblage diagrams with Theriak/Domino software, *Am. Mineral.*, 95, 1006–1016, 2010.
- Evans, K. A., Green, E. C. R., and Powell, R.: Equilibrium and nonequilibrium in metamorphic rocks. In *Treatise on Geochemistry*, 3rd Edn., Elsevier, 2, 571–619, <https://doi.org/10.1016/B978-0-323-99762-1.00112-1>, 2025.
- Feenstra, A., Petrakakis, K., and Rhede, D.: Variscan relicts in Alpine high-P pelitic rocks from Samos (Greece): evidence from multi-stage garnet and its included minerals, *J. Metamorph. Geol.*, 25, 1011–1033, 2007.
- Forshaw, J. B. and Pattison, D. R. M.: Major-element geochemistry of pelites, *Geology*, 51, 39–43, 2023.
- Gabriele, P., Ballèvre, M., Jaillard, E., and Hernandez, J.: Garnet-chloritoid-kyanite metapelites from the Raspas Complex (SW Ecuador): a key eclogite-facies assemblage, *Eur. J. Mineral.*, 15, 977–989, 2003.
- Gaidies, F. and George, F. R.: The interfacial energy penalty to crystal growth close to equilibrium, *Geology*, 49, 988–992, 2021.
- Gaidies, F., Abart, R., de Capitani, C., Schuster, R., Connolly, J. A. D., and Reusser, E.: Characterization of polymetamorphism in the Austroalpine basement east of the Tauern Window using garnet isopleth thermobarometry, *J. Metamorph. Geol.*, 24, 451–475, 2006.
- Gaidies, F., de Capitani, C., Abart, R., and Schuster, R.: Prograde garnet growth along complex P – T – t paths: results from numerical experiments on polyphase garnet from the Wölz Complex (Austroalpine basement), *Contrib. Mineral. Petrol.*, 155, 673–688, 2008.
- Ganne, J., Bussy, F., and Vidal, O.: Multi-stage garnet in the Internal Briançonnais basement (Ambin Massif, Savoy): New petrological constraints of the blueschist-facies metamorphism in the Western Alps and tectonic implications, *J. Petrol.*, 44, 1281–1308, 2003.

- Gasco, I., Gattiglio, M., and Borghi, A.: Lithostratigraphic setting and P – T metamorphic evolution for the Dora Maira Massif along the Piedmont Zone boundary (middle Susa Valley, NW Alps), *Int. J. Earth Sci.*, 100, 1065–1085, 2011.
- George, F. R. and Gaidies, F.: Characterisation of a garnet population from the Sikkim Himalaya: insights into the rates and mechanisms of porphyroblast crystallisation, *Contrib. Mineral. Petrol.*, 172, 57, <https://doi.org/10.1007/s00410-017-1372-y>, 2017.
- George, F. R., Viete, D. R., Guice, G. L., Harvey, K. M., Walker, S., and Baxter, E. F.: Polymetamorphism and metastability in Paleozoic schists of the central Appalachian Baltimore Terrane, USA, *Lithos*, 488–489, 107824, <https://doi.org/10.1016/j.lithos.2024.107824>, 2024.
- Ghignone, S., Scaramuzzo, E., Bruno, M., and Livio, F. A.: A new UHP Unit in the Western Alps: first occurrence of coesite from the Monviso Massif (Italy), *Am. Mineral.*, 108, 1368–1375, 2023.
- Ghignone, S., Gilio, M., Borghini, A., Boero, F., Bruno, M., and Scaramuzzo, E.: Mineralogical and petrological constraints and tectonic implications of a new coesite-bearing unit from the Alpine Tethys oceanic slab (Susa Valley, Western Alps), *Lithos*, 472/473, 107575, <https://doi.org/10.1016/j.lithos.2024.107575>, 2024.
- Gillet, P., Le Cl  ac'h, A., and Madon, M.: High-temperature Raman spectroscopy of SiO_2 and GeO_2 polymorphs: anharmonicity and thermodynamic properties at high temperatures, *J. Geophys. Res.*, 95, 21635–21655, 1990.
- Giuntoli, F., Lanari, P., Burn, M., Kunz, B. E., and Engi, M.: Deeply subducted continental fragments – Part 2: Insight from petrochronology in the central Sesia Zone (western Italian Alps), *Solid Earth*, 9, 191–222, <https://doi.org/10.5194/se-9-191-2018>, 2018.
- Groppo, C.: P – T – X conditions of metamorphic systems, In *Treatise on Geochemistry*, 3rd Edn., Elsevier, 2, 411–446, <https://doi.org/10.1016/B978-0-323-99762-1.00001-2>, 2025.
- Groppo, C., Ferrando, S., Castelli, D., Elia, D., Meirano, V., and Facchinetti, L.: A possible new UHP unit in the Western Alps as revealed by ancient roman Quern-stones from Costigliole Saluzzo, Italy, *Eur. J. Mineral.*, 28, 1215–1232, 2016.
- Groppo, C., Ferrando, S., Gilio, M., Botta, S., Nosenzo, F., Balestro, G., Festa, A., and Rolfo, F.: What's in the sandwich? New P – T constraints from the (U)HP nappe stack of southern Dora-Maira Massif (Western Alps), *Eur. J. Mineral.*, 31, 665–683, 2019.
- Groppo, C., Ferrando, S., Tursi, F., and Rolfo, F.: A new UHP-HP tectono-metamorphic architecture for the southern Dora-Maira Massif nappe stack (western Alps) based on petrologic and microstructural evidence, *J. Metamorph. Geol.*, 43, 359–383, <https://doi.org/10.1111/jmg.12812>, 2025.
- Guillot, S., de Sigoyer, J., Lardeaux J.-M., and Mascle, G.: Eclogitic metasediments from the Tso Moriri area (Ladakh, Himalaya): evidence for continental subduction during India-Asia convergence, *Contrib. Mineral. Petrol.*, 128, 197–212, 1997.
- Guiraud, M., Burg, J.-P., and Powell, R.: Evidence for a Variscan suture zone in the Vend  e, France: a petrological study of blueschist facies rocks from Bois de Cen  , *J. Metamorph. Geol.*, 5, 225–267, 1987.
- Guiraud, M., Powell, R., and Rebay, G.: H_2O in metamorphism and unexpected behaviour in the preservation of metamorphic assemblages, *J. Metamorph. Geol.*, 19, 445–454, 2001.
- Heinrich, C. A.: Kyanite-eclogite to amphibolite facies evolution of hydrous mafic and pelitic rocks, Adula Nappe, Central Alps., *Contrib. Mineral. Petrol.*, 81, 30–38, 1982.
- Hemley, R. J.: Pressure dependence of Raman spectra of SiO_2 polymorphs: α -quartz, coesite, and stishovite, *Geophys. Monogr. Ser.*, 39, 347–359, 1987.
- Henry, C., Michard, A., and Chopin, C.: Geometry and structural evolution of ultra-high pressure and high pressure rocks from the Dora-Maira massif, western Alps, Italy, *J. Struct. Geol.*, 15, 965–981, 1993.
- Holland, T. J. B. and Powell, R.: An internally consistent thermodynamic data set for phases of petrological interest, *J. Metamorph. Geol.*, 16, 309–343, 1998.
- Holland, T. J. B. and Powell, R.: An improved and extended internally consistent thermodynamic dataset for phases of petrological interest, involving a new equation of state for solids, *J. Metamorph. Geol.*, 29, 333–383, 2011.
- Hoschek, G., Konzett, J., and Tessadri, R.: Phase equilibria in quartzitic garnet-kyanite-chloritoid micaschist from the Eclogite Zone, Tauern Window, Eastern Alps, *Eur. J. Mineral.*, 22, 721–732, 2010.
- Jouvent, M., Lexa, O., Peřestý, V., and Jeřábek, P.: New constraints on the tectonometamorphic evolution of the Erzgebirge orogenic wedge (Saxothuringian Domain, Bohemian Massif), *J. Metamorph. Geol.*, 40, 687–715, 2022.
- Katagas, C.: Ferroglaucophane and chloritoid-bearing metapelites from the Phyllite series, southern Peloponnese, Greece, *Mineral. Mag.*, 43, 975–978, 1980.
- Korsakov, A. V., Hutsebaut, D., Theunissen, K., Vandenabeele, P., and Stepanov, A. S.: Raman mapping of coesite inclusions in garnet from the Kokchetav Massif (Northern Kazakhstan), *Spectrochim. Acta A*, 68, 1046–1052, 2007.
- Lanari, P. and Engi, M.: Local bulk composition effects on metamorphic mineral assemblages, *Rev. Mineral. Geochem.*, 83, 55–102, 2017.
- Le Bayon, B., Pitra, P., Ball  vre, M., and Bohn, M.: Reconstructing P – T paths during continental collision using multi-stage garnet (Gran Paradiso nappe, Western Alps), *J. Metamorph. Geol.*, 24, 477–496, 2006.
- L  pez-Carmona, A., Abati, J., and Reche, J.: Petrologic modeling of chloritoid-glaucophane schists from the NW Iberian Massif, *Gondwana Res.*, 17, 377–391, <https://doi.org/10.1016/j.gr.2009.10.003>, 2010.
- L  pez-Carmona, A., Pitra, P., and Abati, J.: Blueschist-facies metapelites from the Malpica-Tui Unit (NW Iberian Massif): phase equilibria modelling and H_2O and Fe_2O_3 influence in high-pressure assemblages, *J. Metamorph. Geol.*, 31, 263–280, 2013.
- Luisier, C., Ball  vre, M., and Duretz, T.: The role of H_2O on metamorphism and deformation at high pressure: a combined petrological and thermo-mechanical study based on the Gran Paradiso Unit, Western Alps, *Lithos*, 446, 107123, <https://doi.org/10.1016/j.lithos.2023.107123>, 2023.
- Manzotti, P., Pitra, P., Langlade, M., and Ball  vre, M.: Constraining P – T condition during thrusting of a higher pressure unit over a lower pressure one (Gran Paradiso, Western Alps), *J. Metamorph. Geol.*, 33, 981–1002, 2015.
- Manzotti, P., Ball  vre, M., and Poujol, M.: Detrital zircon geochronology in the Dora-Maira and Zone Houill  re: A record

- of sediment travel paths in the Carboniferous, *Terra Nova*, 28, 279–288, 2016.
- Manzotti, P., Bosse, V., Pitra, P., Robyr, M., Schiavi, F., and Ballèvre, M.: Exhumation rates in the Gran Paradiso Massif (Western Alps) constrained by in situ U-Th-Pb dating of accessory phases (monazite, allanite and xenotime), *Contrib. Mineral. Petrol.*, 173, 24, <https://doi.org/10.1007/s00410-018-1452-7>, 2018.
- Manzotti, P., Schiavi, F., Nosenzo, F., Pitra, P., and Ballèvre, M.: A journey towards the forbidden zone: a new, cold, UHP unit in the Dora-Maira Massif (Western Alps), *Contrib. Mineral. Petrol.*, 177, 59, <https://doi.org/10.1007/s00410-022-01923-8>, 2022.
- Manzotti, P., Regis, D., Petts D. C., Graziani, R., and Polivchuk, M.: Formation of multistage garnet grains by fragmentation and overgrowth constrained by microchemical and microstructural mapping, *J. Metamorph. Geol.*, 42, 471–496, 2024.
- Manzotti, P., Millonig, L. J., Gerdes, A., Whitehouse, M. J., Jeon, H., Poujol, M., and Ballèvre, M.: Protolith age, and timing of burial and exhumation of the UHP Chasteiran Unit (Dora-Maira Massif, Western Alps), constrained by zircon, garnet and rutile petrochronology, *Lithos*, 496–497, 107951, <https://doi.org/10.1016/j.lithos.2025.107951>, 2025.
- Maldonado, R., Ortega-Gutiérrez, F., and Hernández-Urbe, D.: Garnet-chloritoid-paragonite metapelites from the Chuacús Complex (Central Guatemala): new evidence for continental subduction in the North America-Caribbean plate boundary, *Eur. J. Mineral.*, 28, 1169–1186, 2016.
- Meyre, C., de Capitani, C., Zack, T., and Frey, M.: Petrology of high-pressure metapelites from the Adula Nappe (Central Alps, Switzerland), *J. Petrol.*, 40, 199–213, 1999.
- Michard, A., Schmid, S. M., Lahfid, A., Ballèvre, M., Manzotti, P., Chopin, C., Iaccarino, S., and Dana, D.: The Maira-Sampeyre and Val Grana Allochthons (south Western Alps): review and new data on the tectonometamorphic evolution of the Briançonnais distal margin, *Swiss J. Geosci.*, 115, 19, <https://doi.org/10.1186/s00015-022-00419-8>, 2022.
- Mposkos, E. and Liati, A.: Metamorphic evolution of metapelites in the high-pressure terrane of the Rhodope Zone, Northern Greece, *Can. Mineral.*, 31, 401–424, 1993.
- Nagurney, A. B., Caddick, M. J., Dragovic, B., and Busse, K.: The (chemical) potential for understanding overstepped garnet nucleation and growth, *Am. Mineral.*, 106, 812–829, 2021.
- Negulescu, E., Săbău, G., and Massonne, H.-J.: Growth of chloritoid and garnet along a nearly isothermal burial path to 70 km depth: an example from the Bughea Metamorphic Complex, Leaota Massif, South Carpathians, *Min. Pet.*, 112, 535–553, 2018.
- Nerone, S., Petroccia, A., Caso, F., Dana, D., and Maffei, A.: Assessing the importance of H₂O content in the tectonometamorphic evolution of shear zones: A case study from the Dora-Maira Massif (Western Alps), *J. Metamorph. Geol.*, 42, 171–196, 2024.
- Nosenzo, F., Manzotti, P., Poujol, M., Ballèvre, M., and Langlade, J.: A window into an older orogenic cycle: *P–T* conditions and timing of the pre-Alpine history of the Dora-Maira Massif (Western Alps), *J. Metamorph. Geol.*, 40, 789–821, 2022.
- Nosenzo, F., Manzotti, P., and Robyr, M.: H₂O budget and metamorphic re-equilibration in polycyclic rocks as recorded by garnet textures and chemistry, *Lithos*, 452–453, 107230, 2023.
- Nosenzo, F., Manzotti, P., Krona, M., Ballèvre, M., and Poujol, M.: Tectonic architecture of the northern Dora-Maira Massif (Western Alps, Italy): field and geochronological data, *Swiss J. Geosci.*, 117, 6, <https://doi.org/10.1186/s00015-024-00459-2>, 2024.
- Novarese, V.: I giacimenti di grafite delle Alpi Cozie, *Boll. R. Com. Geol. Italia*, 29, 3–35, 1898.
- Okay, A., Xu, S. T., and Sengör, A. M. C.: Coesite from the Dabie Shan eclogites, central China, *Eur. J. Mineral.*, 1, 595–598, 1989.
- Orozbaev, R., Hirajima, T., Bakirov, A., Takasu, A., Maki, K., Yoshida, K., Sakiev, K., Bakirov, A., Hirata, T., Tagiri, M., and Togonbaeva, A.: Trace element characteristics of clinzoisite pseudomorphs after lawsonite in talc-garnet-chloritoid schists from the Makbal UHP Complex, northern Kyrgyz Tian-Shan, *Lithos*, 226, 98–115, 2015.
- Parkinson, C. D.: Coesite inclusions and prograde compositional zonation of garnet in whiteschist of the Hp-UHPM Kokchetav massif, Kazakhstan: a record of progressive UHP metamorphism, *Lithos*, 52, 215–233, 2000.
- Pattison, D. R. M. and Tinkham, D. K.: Interplay between equilibrium and kinetics in prograde metamorphism of pelites: An example from the Nelson aureole, British Columbia, *J. Metamorph. Geol.*, 27, 249–279, 2009.
- Pattison, D. R. M., de Capitani, C., and Gaidies, F.: Petrological consequences of variations in metamorphic reaction affinity, *J. Metamorph. Geol.*, 29, 953–977, 2011.
- Petroccia, A. and Iaccarino, S.: Metacglomerate in the Pinerolo Unit (Dora Maira Massif, Western Alps): a key outcrop for Alpine geology and training structural geologists, *Int. J. Earth Sci.*, 111, 317–319, 2022.
- Powell, R. and Holland, T. J. B.: Calculated mineral equilibria in the pelite system, KFMASH (K₂O–FeO–MgO–Al₂O₃–SiO₂–H₂O), *Am. Mineral.*, 75, 367–380, 1990.
- Powell, R. and Holland, T.: Using equilibrium thermodynamics to understand metamorphism and metamorphic rocks, *Elements*, 6, 309–314, 2010.
- Proyer, A.: The preservation of high-pressure rocks during exhumation: metagranites and metapelites, *Lithos*, 70, 183–194, 2003.
- Regis, D., Rubatto, D., Darling, J., Cenki-Tok, B., Zucali, M., and Engi, M.: Multiple metamorphic stages within an eclogite-facies terrane (Sesia Zone, Western Alps) revealed by Th-U-Pb petrochronology, *J. Petrol.*, 55, 1429–1456, 2014.
- Reinecke, T.: Very-high pressure metamorphism and uplift of coesite-bearing metasediments from the Zermatt-Saas zone, Western Alps, *Eur. J. Mineral.*, 3, 7–17, 1991.
- Reinecke, T.: Prograde high- to ultrahigh-pressure metamorphism and exhumation of oceanic sediments at Lago di Cignana, Zermatt-Saas Zone, western Alps, *Lithos*, 42, 147–189, 1998.
- Ridley, J. and Thompson, A. B.: The role of mineral kinetics in the development of metamorphic microtextures, in: Fluid-rock interactions during metamorphism, edited by: Walther, J. V. and Wood, B. J., 154–193, Springer, New York, <https://doi.org/10.1007/978-1-4612-4896-5>, 1986.
- Rubie, D. C.: The catalysis of mineral reactions by water and restrictions on the presence of aqueous fluid during metamorphism, *Mineral. Mag.*, 50, 399–415, <https://doi.org/10.1180/minmag.1986.050.357.05>, 1986.
- Santoro, L., Bertone, V., Ferrando, S., and Groppo, C.: New insights into graphite deposits in Chisone and Germanasca

- valleys (Dora-Maira Massif, Western Italian Alps): scientific advances and applied perspectives, *Minerals*, 15, 455, <https://doi.org/10.3390/min15050455>, 2025.
- Scailliet, S., Féraud, G., Ballèvre, M., and Amouric, M.: Mg/Fe and [(Mg,Fe)Si-Al₂] compositional control on argon behaviour in high-pressure white micas: A ⁴⁰Ar / ³⁹Ar continuous laser-probe study from the Dora-Maira nappe on the internal western Alps, Italy, *Geochim. Cosmochim. Ac.*, 56, 2851–2872, 1992.
- Schorn, S.: Dehydration of metapelites during high-P metamorphism: the coupling between fluid sources and fluid sinks, *J. Metamorph. Geol.*, 36, 369–391, 2018.
- Schorn, S.: Self-induced incipient “eclogitization” of metagranitoids at closed system conditions, *J. Metamorph. Geol.*, 40, 1271–1290, 2022.
- Schulte, B. and Blümel, P.: Metamorphic evolution of eclogite and associated garnet-mica schist in the high-pressure metamorphic Maksyutov Complex, Ural, Russia, *Geol. Rund.*, 87, 561–576, 1999.
- Sharma, S. K., Mammone, J. F., and Nicol, M. F.: Raman investigation of ring configurations in vitreous silica, *Nature*, 292, 140–141, 1981.
- Smith, D. C.: Coesite in clinopyroxene in the Caledonides and its implications for geodynamics, *Nature*, 310, 641–644, 1984.
- Smye, A. J., Greenwood, L. V., and Holland, T. J. B.: Garnet-chloritoid-kyanite assemblages: eclogite facies indicators of subduction constraints in orogenic belts, *J. Metamorph. Geol.*, 28, 753–768, 2010.
- Spear, F. S.: Garnet growth after overstepping, *Chem. Geol.*, 466, 491–499, <https://doi.org/10.1016/j.chemgeo.2017.06.038>, 2017.
- Spear, F. S. and Pattison, D. R. M.: The implications of overstepping for metamorphic assemblage diagrams (MADs), *Chem. Geol.*, 457, 38–46, 2017.
- Szczepański, J., Zhon, X., Dąbrowski, M., Wang, H., and Golén, M.: Combined phase diagram modelling and quartz-in-garnet barometry of HP metapelites from the Kamieniec Metamorphic Belt (NE Bohemian Massif), *J. Metamorph. Geol.*, 40, 3–37, 2022.
- Taguchi, T., Kouketsu, Y., Ygami, Y., Kobayashi, T., and Miyake, A.: Hidden intact coesite in deeply subducted rocks, *Earth Planet. Sc. Lett.*, 558, 116763, <https://doi.org/10.1016/j.epsl.2021.116763>, 2021.
- Tamang, S., Groppo, C., Girault, F., and Rolfo, F.: Implications of garnet nucleation overstepping for the *P–T* evolution of the Lesser Himalayan Sequence of central Nepal, *J. Metamorph. Geol.*, 41, 271–297, 2023.
- Tenczer, V., Powell, R., and Stüwe, K.: Evolution of H₂O content in a polymetamorphic terrane: the Plattengneiss Shear Zone (Koralpe, Austria), *J. Metamorph. Geol.*, 24, 281–295, 2006.
- Thompson, A. B. and Connolly, J. A. D.: Metamorphic fluids and anomalous porosities in the lower crust, *Tectonophysics*, 182, 47–55, 1990.
- Tinkham, D. and Ghent, E.: Estimating *P–T* conditions of garnet growth with isochemical phase-diagram sections and the problem of effective bulk composition, *Can. Mineral.*, 43, 35–50, 2005.
- Tinkham, D., Zuluaga, C. A., and Stowell, H.: Metapelite equilibria modelling in MnNCKFMASH: the effect of variable Al₂O₃ and MgO / (MgO + FeO) on mineral stability, *Geol. Material. Res.*, 3, 1–42, 2001.
- Vuichard, J.-P. and Ballèvre, M.: Garnet-chloritoid equilibria in eclogitic pelitic rocks from the Sesia zone (Western Alps): their bearing on phase relations in high pressure metapelites, *J. Metamorph. Geol.*, 6, 135–157, 1988.
- Wain, A.: New evidence for coesite in eclogite and gneisses: defining an ultrahigh-pressure province in the Western Gneiss region of Norway, *Geology*, 25, 927–930, 1997.
- Waters, D. J. and Lovegrove, D. P.: Assessing the extent of disequilibrium and overstepping of prograde metamorphic reactions in metapelites from the Bushveld Complex aureole, South Africa, *J. Metamorph. Geol.*, 20, 135–149, 2002.
- Wei, C. J. and Song, S. G.: Chloritoid-glaucophane schist in the north Qilian orogen, NW China: phase equilibria and *P–T* path from garnet zonation, *J. Metamorph. Geol.*, 26, 301–316, 2008.
- Yang, P. and Rivers, T.: Chromium and manganese zoning in pelitic garnet and kyanite: spiral, overprint, and oscillatory (?) zoning patterns and the role of growth rate, *J. Metamorph. Geol.*, 19, 455–474, 2001.
- Žáčková, E., Konopásek, J., Jeřábek, P., Finger, F., and Košler, J.: Early Carboniferous blueschist facies metamorphism in metapelites of the West Sudetes (Northern Saxothuringian Domain, Bohemian Massif), *J. Metamorph. Geol.*, 28, 361–379, 2010.
- Zuluaga, C. A., Stowell, H. H., and Tinkham, D. K.: The effect of zoned garnet on metapelites pseudosection topology and metamorphic *P–T* paths, *Am. Mineral.*, 90, 1619–1628, 2005.